Visual Neuroscience (1995), **12**, 951–970. Printed in the USA.

Two signals in the human rod visual system: A model based on electrophysiological data

ANDREW STOCKMAN,[1] LINDSAY T. SHARPE,[2] KLAUS RÜTHER,[3] AND KNUT NORDBY[4]

[1]Department of Psychology, University of California San Diego, La Jolla
[2]Forschungsstelle für Experimentelle Ophthalmologie, University of Tübingen, D-72076 Tübingen, Germany
[3]Pathophysiologie des Sehens und Neuro-Ophthalmologie, Universitäts-Augenklinik, University of Tübingen, D-72076 Tübingen, Germany
[4]Norwegian Telecommunications Administration, Research Department, N-2007 Kjeller, Norway

(RECEIVED October 5, 1994; ACCEPTED March 23, 1995)

Abstract

In the human rod visual system, self-cancellation of flicker signals is observed at high rod intensity levels near 15 Hz, both perceptually and in the electroretinogram (ERG). This and other evidence suggests that two rod signals are transmitted through the human retina with different speeds of transmission. Here we report a series of flicker ERG recordings from a normal observer and an observer who lacks cone vision. From these results, we propose a quantitative model of the two rod signals, which assumes (1) that the amplitude of the slow signal grows linearly with log intensity but then saturates at ~1 scot. td; (2) that the amplitude of the fast signal grows linearly with intensity; (3) that there is a difference in time delay of ~33 ms between two rod signals of the same polarity (or of ~67 ms if the signals are of inverted polarity); and (4) that the time delay of both signals declines linearly with log intensity (by ~10 ms per log scot. td). These simple assumptions provide a remarkably good account of the experimental data. Our results and model are relevant to current anatomical theories of the mammalian rod visual system. We speculate that the slower signal in the human ERG may reflect the transmission of the rod response *via* the rod bipolars and the AII amacrine cells, while the faster signal may reflect its transmission *via* the rod–cone gap junctions and the cone bipolars. There are, however, several objections to this simple correspondence.

Keywords: Flicker, Rods, Scotopic vision, ERG, Electroretinogram, Achromat, Vision and visual sensitivity

Introduction

There is now much accumulated anatomical and physiological evidence that suggests mammalian rods transmit their signals over at least two retinal pathways (see, for example, Kolb & Nelson, 1983; Sterling et al., 1986; Daw et al., 1990; Wässle & Boycott, 1991). One pathway, which is thought to be active mainly at low, scotopic intensities, is from rods to rod bipolars, to AII amacrine cells, and then either to depolarizing cone bipolars and ganglion cells by way of gap junctions or to hyperpolarizing cone bipolars and ganglion cells by way of conventional synapses (Kolb & Famiglietti, 1974; Famiglietti & Kolb, 1975; Kolb, 1977, 1979; Nelson, 1977, 1982; Kolb & Nelson, 1983, 1984; Dacheux & Raviola, 1986; Sterling et al., 1986; Müller et al., 1988; Sterling et al., 1988; Chun et al., 1993). The second pathway, which is thought to be active at higher intensity levels, relies upon gap junctions between rod and cone axon terminals (Kolb, 1977), through which rod signals have direct access to ON and OFF cone bipolars and then to ON and OFF ganglion cells (Nelson, 1977; Nelson & Kolb, 1983).

The duality is believed to apply to all mammalian species (Daw et al., 1990), though the evidence cited to support it comes mainly from physiological and anatomical experiments made in the rat, cat, and rabbit. This wholly ignores much earlier evidence for a duality of the rod system, which comes from perceptual experiments carried out on human observers. More than 50 years ago, Hecht and his co-workers (1938) demonstrated that the highest rate of flicker that could just be perceived with rod vision (the scotopic "critical flicker fusion frequency" or CFF) grows in two distinct stages as the intensity of the flickering light is increased (Hecht et al., 1938, 1948). In the first stage, the CFF rises from low frequencies to reach an asymptote at 15 Hz (or less), where it remains, until, in the second stage, at high scotopic levels [> ~1 scotopic troland (scot. td)], it rises again to reach frequencies as high as 28 Hz (see Conner & MacLeod, 1977; Hess & Nordby, 1986; and also Alpern et al., 1960; Blakemore & Rushton, 1965).

The existence of two stages in the scotopic CFF *vs.* intensity curve implies a duality in the control of rod signals; and this implication is strongly supported by additional experiments

Reprint requests to: Andrew Stockman, Department of Psychology, University of California San Diego, 9500 Gilman Drive, La Jolla, CA 92093-0109, USA.

in which flicker thresholds (Conner, 1982; Sharpe et al., 1989) or flicker delays (Sharpe et al., 1989) are measured as a function of flicker frequency and/or intensity. Compelling support for the duality comes from the flicker threshold measurements, which demonstrate the existence of an intensity region, well above the conventional flicker threshold, within which 15 Hz rod flicker becomes paradoxically invisible or nulled (Sharpe et al., 1989; see also Conner, 1982). This phenomenon, which occurs only near 15 Hz, is depicted in Fig. 1.

Psychophysical estimates of the delay of rod flicker relative to cone flicker reveal that at 15 Hz the rod flicker signal measured just below the null region is delayed by a half-cycle relative to the rod signal measured just above the null region (Sharpe et al., 1989). The presence of two rod signals in opposite phase suggests that the most likely cause of the perceptual null of Fig. 1 is flicker self-cancellation due to destructive interference (see Fig. 2, middle). To explain why the destructive interference occurs near 15 Hz, it need only be assumed that there

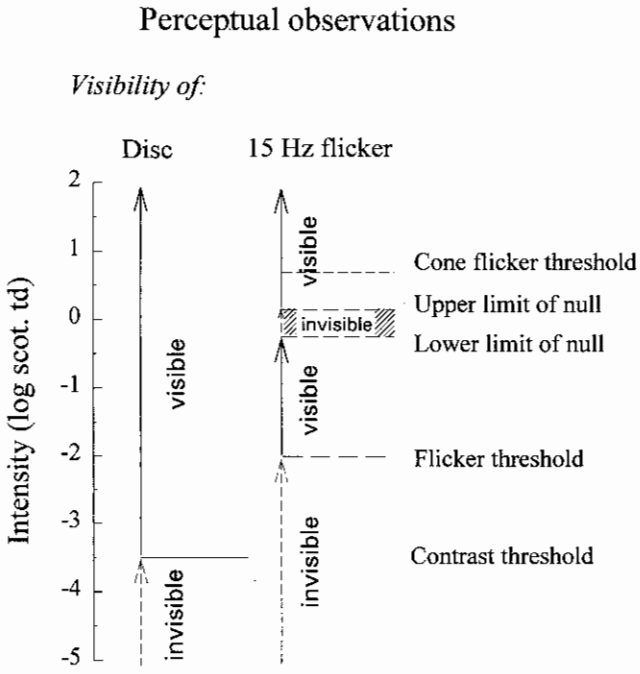

Fig. 1. How increasing the intensity of a disc of light flickering at 15 Hz affects the visibility of the disc (left, vertical arrows) and the visibility of the flicker (right, vertical arrows). At very low intensity levels, neither the disc nor flicker can be detected. As the intensity is increased, the disc becomes visible as the *contrast threshold* is crossed, but it appears steady and non-flickering until the *flicker threshold* is crossed. Unexpectedly, at 15 Hz the flicker (but not the disc) disappears at an intensity above the flicker threshold (the *lower limit of null*) and then reappears again at a still higher intensity (the *upper limit of null*). Since the flicker null region between these limits (hatched area) occurs below the *cone flicker threshold*, it must be a property of rod vision, a conclusion which is confirmed by the finding that the null is found in an achromat (author KN) who lacks functioning cone vision (Stockman et al., 1991). The limits shown here are representative observations based on results in several normal subjects viewing a 500 nm, 6-deg diameter target flickering at 15 Hz and presented at an eccentricity of 13 deg in the peripheral, temporal retina (for example, Sharpe et al., 1989). Comparable observations are obtained with larger fields, such as the Ganzfeld used in this study.

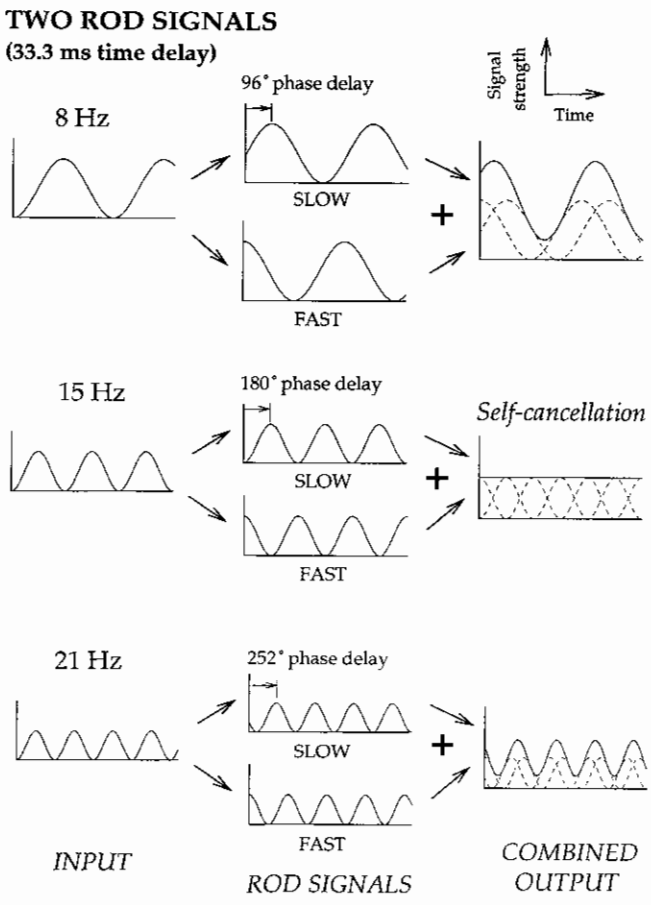

Fig. 2. A theoretical depiction of the interaction between the slow and fast rod signals for three of the flicker rates used in the ERG recordings: 8 Hz (top panels), 15 Hz (middle panels), and 21 Hz (bottom panels). The flicker signal produced by a single stimulus (left column, labeled *INPUT*) is assumed to give rise to a slow and a fast rod signal (middle column, labeled *ROD SIGNALS*). At each frequency, the slower signal is assumed to lag the fast signal by a time delay of 33.3 ms, which is equivalent to a phase delay of 96 deg at 8 Hz, 180 deg at 15 Hz, and 252 deg at 21 Hz. The signals emerging from the two pathways are assumed to be recombined (right column, labeled *COMBINED OUTPUT*) before being transmitted to later stages of the visual system (the original components are shown as dashed curves). For ease of exposition, the two signals are assumed to be equal in magnitude at each frequency. Consequently, at 15 Hz the two signals cancel each other to produce a steady, non-flickering output signal. At other frequencies, the combined signal is of the same frequency as the input and of intermediate phase delay. (The decline in the magnitude of the input signals with frequency represents the rapid decline in rod sensitivity with frequency.)

is a time delay of 33.3 ms between the two signals. Such a delay gives rise to a half-cycle (180 deg) phase delay at 15 Hz (Fig. 2, middle), but produces smaller phase delays at lower frequencies (96 deg at 8 Hz, Fig. 2, top) and larger phase delays at higher frequencies (252 deg at 21 Hz, Fig. 2, bottom) [See eqn (8a), in Appendix]; thus self-cancellation is maximal at 15 Hz. To explain why the null is restricted to a small intensity range (see Fig. 1), it need only be assumed that the relative sizes of the slow and fast rod signals change with intensity, such that the fast signal is smaller than the slow signal below the null,

approximately equal to it within the null, and larger than it above the null.

The effect of increasing the size of the fast signal relative to the slow is illustrated for a time delay of 33.3 ms at 8 and 15 Hz in Fig. 3. In each panel, the amplitude of the slow signal is fixed, while the amplitude of the fast signal is increased from 0 to 8 times the slow signal. Indicated to the left of each function is the ratio of the slow to fast signal size.

At 8 Hz (Fig. 3a) adding the fast signal simply increases the size of the combined output signal and advances its phase (i.e. the peaks move leftward). At 15 Hz (Fig. 3b), the situation is more complicated because the fast signal cancels the slow one, so that the addition of the fast signal reduces the combined output signal, causing it to fall to zero when the two signals are equal (1:1). Also illustrated in Fig. 3 are the relative phase lags (Fig. 3c) and relative amplitudes (Fig. 3d) of the output signals shown in Figs. 3a and 3b plotted as a continuous function of the log ratio of the slow to fast signal size. Notice, in particular, that the phase of the 15 Hz combined output signal (Fig. 3c) abruptly reverses when the two signals are equal and the amplitude is zero (Fig. 3d). In contrast, the phase and amplitude of the 8 Hz combined output signal change gradually.

If the size of the fast signal relative to the slow signal grows steadily with intensity, then a perfect null should occur only at the intensity at which the two 15 Hz rod signals are precisely equal. The perceptual null, however, spans a range of intensities of about 0.5 $\log_{10}$ unit (Fig. 1). This is explicable if we make the additional assumption that the final (combined) output signal must exceed a certain threshold size before it is detected (e.g. a threshold size of ~0.5 relative amplitude units might be assumed in the example shown in Fig. 3d).

Although these assumptions adequately explain the most prominent features of the psychophysical and electrophysiological results, such as the flicker null and the 180 deg phase shift at 15 Hz (see Sharpe et al., 1989; Stockman et al., 1991), they do not permit any predictions about the dependence of the slow and fast rod signals on intensity, nor about the dependence of the rod phase delay on intensity (except at the null frequency at which the change should be abrupt—as at 15 Hz in Fig. 3c). To overcome this limitation, we have made a series of ERG recordings in the normal and the achromat observer at frequencies ranging from 8 to 21 Hz, and at adaptation levels ranging from low to high scotopic intensities. These new recordings support the basic assumptions, and they allow us to model the way in which the rod flicker ERG depends on intensity. Moreover, the recordings and the resulting model provide insight into how the two rod signals in the human may relate to the rod pathways anatomically and physiologically identified in the mammalian retina.

Material and Methods

Subjects

A normal, male trichromat (author, LTS) and a male achromat (author, KN) served as the main observers in this study. The normal observer was slightly myopic (−2 diopters) with normal color vision as indicated by conventional acuity and color vision tests. The achromat observer (KN) displayed all of the classic symptoms of typical, complete achromatopsia (rod monochromacy) and has been consistently shown to lack functioning cone vision (Hess & Nordby, 1986; Sharpe et al., 1986; Nordby & Sharpe, 1988; Sharpe & Nordby, 1990). He is hyperopic (+9.0 diopters). For the Ganzfeld (full-field) flicker ERG recordings reported in this paper, corrective lenses were not required.

Apparatus and stimuli

The test flashes for the scotopic ERG measurements were generated by a standard Ganzfeld stimulator (LKC Technologies, Inc., Gaithersburg, MD). Stimulus and recording conditions were in accordance with the ERG standard established by the International Society for Clinical Electrophysiology of Vision (Marmor et al., 1989). The subject, positioned with the aid of a headrest, stared into the center of a Ganzfeld bowl. The bowl was homogeneously illuminated by white flashes produced by a Xenon discharge lamp [correlated color temperature ~6000 K; see Wyszecki & Stiles (1982), Table 1(2.4.4)]. Each flash was triggered by a computer (LKC Universal Testing and Analysis System-Electrophysiology 2000), which was also used to store and analyze the ERG recordings. The duration of the flashes was less than 10 μs at half-maximum intensity. Flicker was obtained by repeating the flash at the required rate. The flicker yielded by this device was full-field at 100% contrast. The flash luminance was controlled by the interposition of gelatin neutral density filters (Kodak, Wratten).

The time-averaged photopic luminances in cd/m^2 were measured at each frequency with the use of an integrating spectroradiometer (Model #PR-704, SpectraScan Fast Spectral Scanning SpectraRadiometer, Photo Research, Chatsworth, CA). We then converted those values to photopic trolands by assuming a dilated pupil size of 7.5 mm (see Nordby & Sharpe, 1988 and Wyszecki & Stiles, 1982), and finally to scotopic trolands (scot. td) by using the appropriate value in Table 1(2.4.4) of Wyszecki and Stiles (1982) for a blackbody radiator of 6000 K. (Values in log scot. cd/m^2 can be obtained by subtracting 1.65 from the log scot. td values). All neutral density filters were calibrated *in situ*.

Procedure

Before beginning an experiment, each subject dark-adapted for 45 min. The subject's pupils were dilated with 0.5% tropicamide, and fiber electrodes (DTL) were placed on the conjunctiva of each eye near the corneal border. Reference electrodes (Ag–AgCl) were placed over both temporal bones and a ground electrode was placed on the forehead. The ERG responses to the flashes were recorded and stored by means of the LKC computer. To avoid the effects of the rapid changes in gain in the rod system that accompany the onset of flickering lights (e.g. Dodt & Walther, 1958, Fig. 2), we discarded the responses to the flashes presented during the first 2 s. The signals were filtered to remove responses that were too low (<1 Hz) or too high (>30 Hz) in frequency, and averaged 50 times on line. During these short exposures, we found no systematic increase in the amplitude of the flicker response, such as would be expected for longer exposures of cone flicker at high intensities (e.g. Peachey et al., 1992). The measurements were repeated until at least two clearly reproducible responses were obtained. These were later base-line corrected and averaged off-line. Average recordings obtained at 8 and 15 Hz are reproduced in Figs. 4 and 5, respectively.

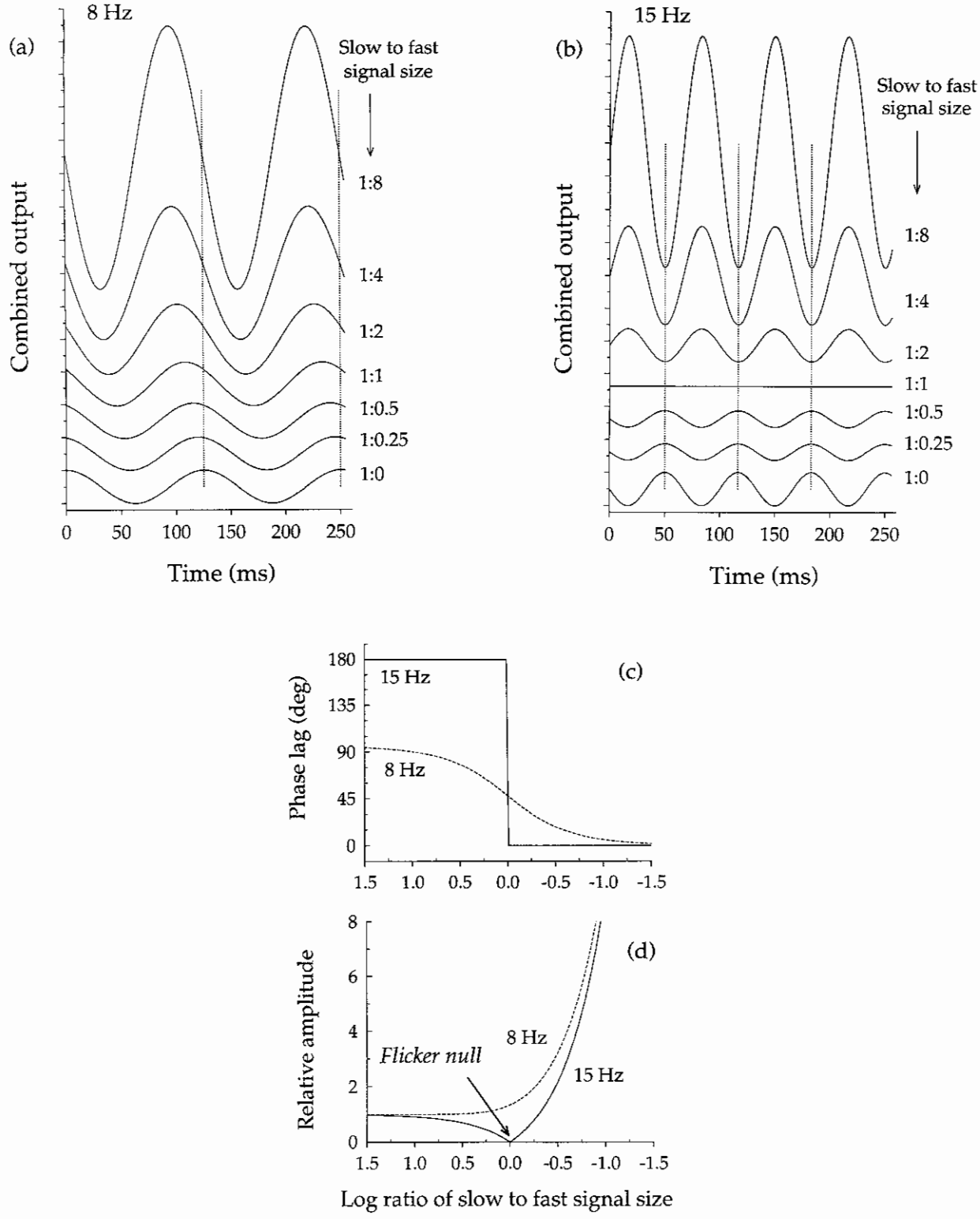

Fig. 3. Illustrations at 8 Hz and 15 Hz of the effect on the output signal of adding a fast rod signal that increases in size relative to a slow signal that is fixed in size. As in Fig. 2, the phase delay between the signals is assumed to be 33.3 ms (i.e. 96 deg at 8 Hz and 180 deg at 15 Hz). (a) shows the 8-Hz output signal and (b) the 15-Hz output signal. The lowest curves in (a) and (b) represent the pure slow rod signal (a slow to fast signal ratio of 1:0), while the other curves represent the fast rod signal added to the slow rod signal in strengths increasing upwards from 0.25 to 8 times the slow signal. The vertical dotted lines mark the peaks of the pure slow signal. Also illustrated are the dependence of the relative phase lag (c) and the relative amplitude (d) of the combined output signal at 8 Hz (dashed lines) and 15 Hz (continuous lines) on the logarithmic ratio of the slow to fast signal size.

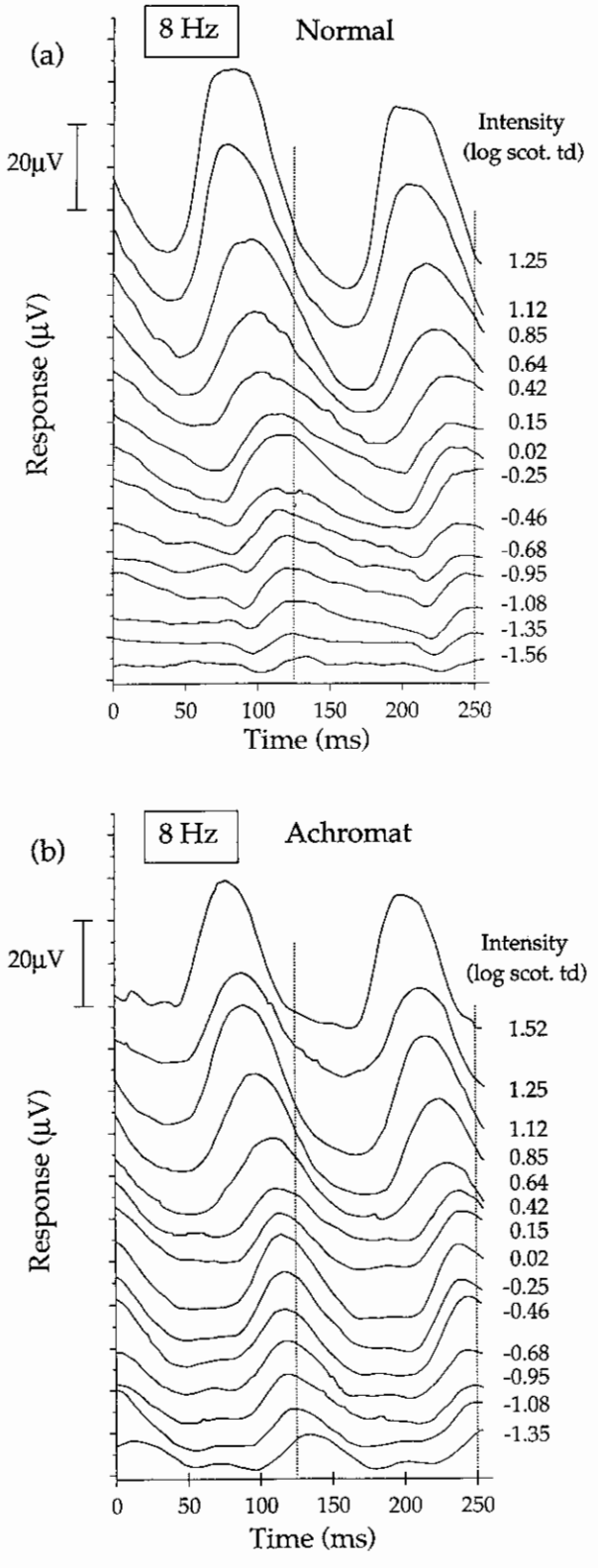

Fig. 4. Ganzfeld electroretinogram recordings at 8 Hz for the normal (a) and achromat (b) observer. In each panel, the time-averaged flicker intensity increases upwards in steps of approximately 0.2 $\log_{10}$ unit intensity levels ranging from −1.56 to 1.25 $\log_{10}$ scot. td (a) or from −1.35 to 1.52 $\log_{10}$ scot. td (b). The intensity in $\log_{10}$ scot. td is noted to the right of each record. The vertical dotted lines demonstrate that there is a continuous phase shift with increasing flicker intensity.

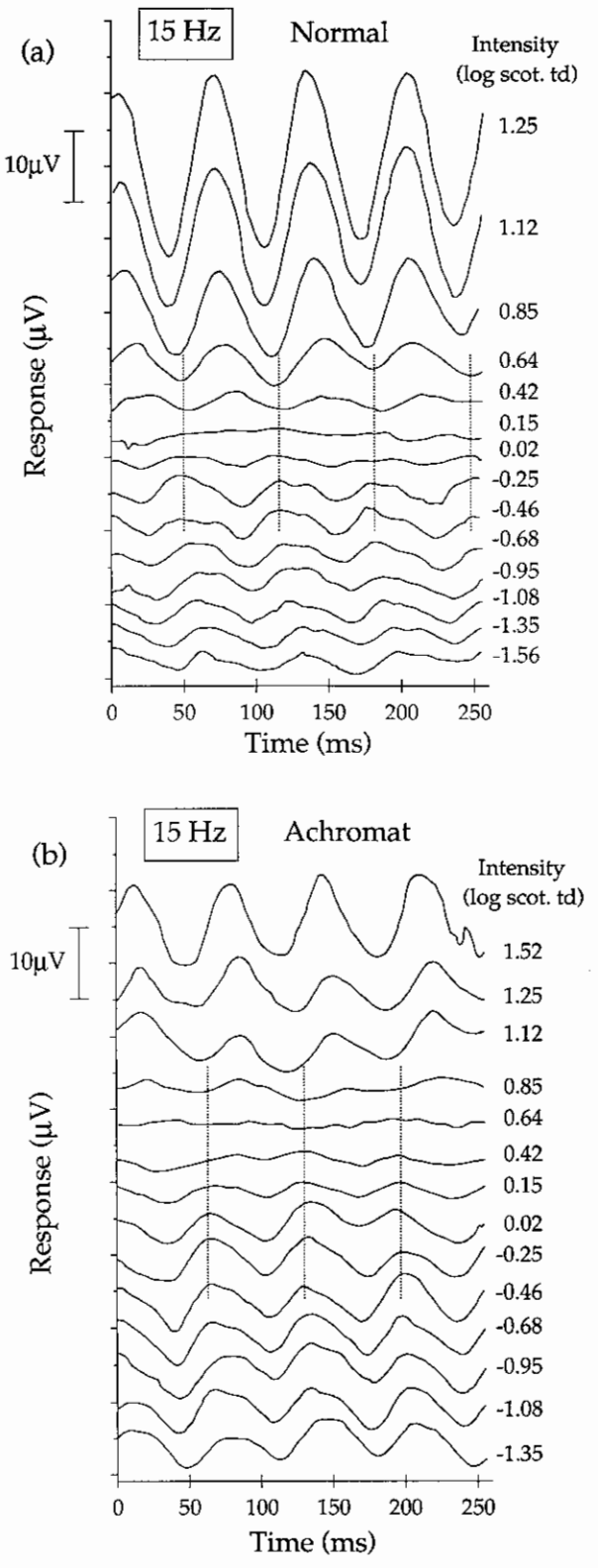

Fig. 5. Ganzfeld electroretinogram recordings at 15 Hz for the normal (a) and achromat (b) observer. The vertical dotted lines demonstrate how the phase abruptly changes by 180 deg between the flicker luminances immediately above and below the flicker null (~0.15 $\log_{10}$ scot. td for the normal and ~0.64 $\log_{10}$ scot. td for the achromat). The vertical scale is approximately twice that for the 8-Hz records. Other details are as for Fig. 4.

Cone intrusion

A small cone response will contribute to the ERG in the normal observer, but not in the rod monochromat, at the three highest levels employed. Compared with the rod responses at these levels, however, the cone responses are small. Measurements in two observers with congenital stationery nightblindness, who lack rod but not cone ERG responses, confirm that the cone response at these levels is minimal. Accordingly, we have ignored the cone responses in our analysis. As we have demonstrated before, cone responses play little or no role in producing the null or phase reversal (see Fig. 3 of Stockman et al., 1991).

Results

8 and 15 Hz ERG responses

Figs. 4 and 5 show the ERG responses to 8 and 15 Hz Ganzfeld flicker, respectively, in the normal observer (Figs. 4a and 5a) and in the achromat observer (Figs. 4b and 5b). In each panel, the responses have been arranged vertically so that the intensity level, which is given in $\log_{10}$ scotopic trolands to the right of each record, increases upwards.

The form of the results at 8 Hz and at 15 Hz compares well with previous recordings reported for the same two observers (Stockman et al., 1991) and accords with the model predictions illustrated in Fig. 3. In general, at 8 Hz (Fig. 4) the ERG response grows steadily in amplitude with intensity, and its phase advances. (The exception to this generalization is the small decrease in amplitude that can be seen at 0.15 and 0.42 $\log_{10}$ scot. td in the achromat (Fig. 4b) and, to a lesser extent, in the normal (Fig. 4a); this decrease is discussed below.) In contrast, at 15 Hz (Fig. 5) the ERG response falls to a minimum at the same intensity at which the flicker percept vanishes (0.15 $\log_{10}$ scot. td for the normal, and between 0.42 and 0.64 $\log_{10}$ scot. td for the achromat) and its phase abruptly reverses as the null intensity is crossed. The coincidence of the minimum in the ERG with the perceptual null is important because it suggests that the electrical cancellation measured electrophysiologically and the neural cancellation measured perceptually are manifestations of the same phenomenon (see Discussion).

Phase and amplitude of the ERG responses

In addition to the recordings made at 8 and 15 Hz, a series of recordings were made at 11, 14, 16, 17, 18, and 21 Hz in the normal and at 11, 13, 14, 16, 17, and 18 Hz in the achromat. We analyzed all recordings using a Fourier transform to derive the phase and amplitude of the ERG response at each flicker frequency. The results of this analysis are shown in Fig. 6 for

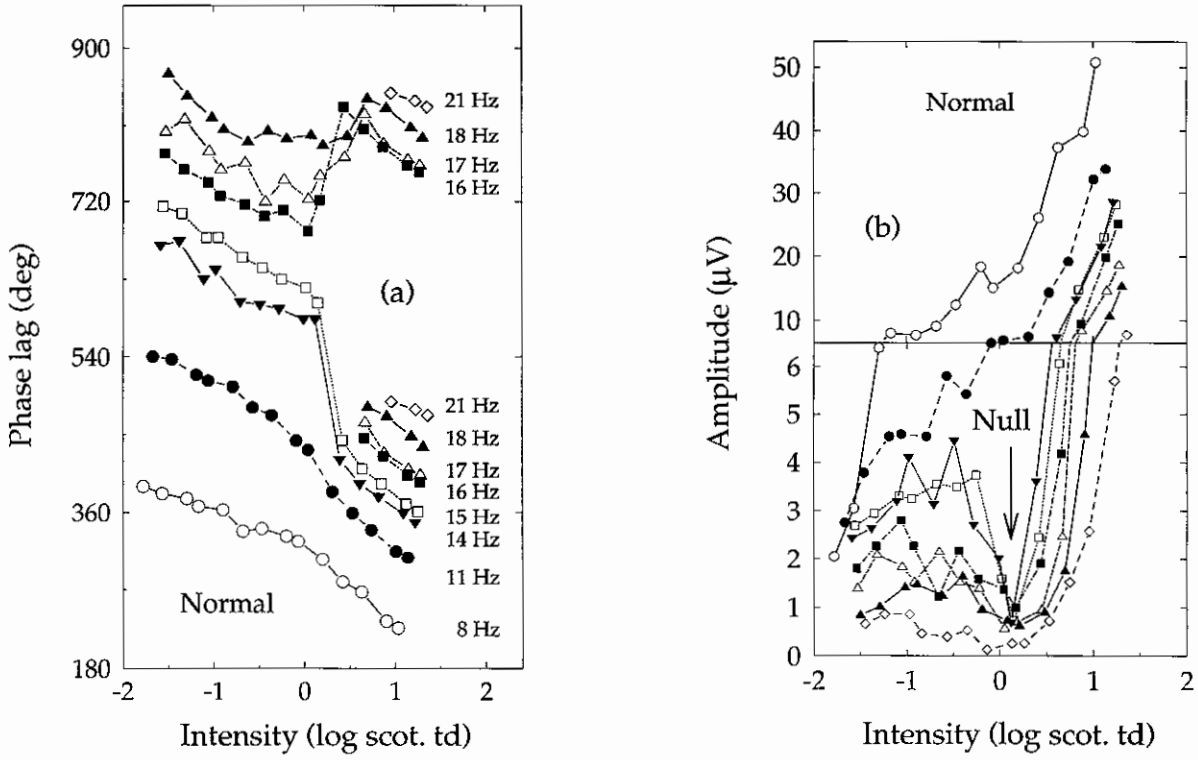

Fig. 6. The phase (a) and amplitude (b) of the ERG response for the normal observer obtained from the original records by means of a Fourier Transform. In panel (a), the phase lags at 16–21 Hz above the null are plotted twice. The lower group are the correct, absolute phase delays; the upper group have been delayed by an additional cycle (see text for details). In panel (b), there is a scale change along the amplitude axis (between 6 and 10 μV) indicated by the continuous line. In this and the subsequent figures, the following symbols are used: open circles (8 Hz); filled circles (11 Hz); open inverted triangles (13 Hz, used for the achromat only); filled inverted triangles (14 Hz); open squares (15 Hz); filled squares (16 Hz); open triangles (17 Hz); filled triangles (18 Hz); and open diamonds (21 Hz). Missing phase lag values indicate that the ERG signal was too small to yield a reliable phase estimate.

the normal observer and in Fig. 7 for the achromat. The 21 Hz ERG responses in the normal observer were too small to yield reliable phase information at lower intensities.

Phase delay

For both the normal (Fig. 6a) and achromat (Fig. 7a) observers, the change in phase delay with intensity appears to have two components: a gradual reduction in phase delay that occurs at all frequencies (see Premise #6 of the Model, below) and a more rapid change centered on 14 or 15 Hz. The rapid change is roughly consistent with a reduction in time delay in going from the slow to the fast rod signal (see Premise #5 of the Model). It occurs at an intensity of ~0.2 $\log_{10}$ scot. td and reaches a maximum of 180 deg at a frequency of ~15 Hz in the normal (corresponding to a time delay of ~33.3 ms); and it occurs at an intensity of ~0.5 $\log_{10}$ scot. td and reaches a maximum of 180 deg at a frequency of ~14 Hz in the achromat (corresponding to a time delay of ~35.7 ms). A comparable difference in the time delay between the two rod signals for these two observers has been reported before (Stockman et al., 1991).

In Figs. 6a and 7a, the phase lags at lower frequencies decrease as the null intensity is crossed, yet those at higher frequencies apparently increase. Though this result seems counterintuitive, it is not. It is entirely consistent with a change from a slow signal to a second, faster signal that precedes it either by 33.3 ms in the normal or by 35.7 ms in the achromat. The apparent increase in phase delay at higher frequencies, despite a reduction in time delay, occurs because flicker is cyclical. When the slow signal lags the fast by 180–360 deg, any given cycle of the slow flicker waveform is closer in phase to the cycle of the fast flicker waveform that originated a cycle later than to the cycle that originated at the same time. Thus, as the fast signal is added to the slow signal, the peak of the resultant waveform moves towards the peak on the fast flicker waveform that originated a cycle later; so that the resultant waveform appears to become more delayed. To show both the apparent phase change and the actual phase lag at higher frequencies in Figs. 6a and 7a, we have plotted the phase lag at intensities above the null twice. The lower group of phase lags at 16–21 Hz in Fig. 6a and at 15–18 Hz in Fig. 7a are the absolute phase lags of the fast rod signal. The upper group have been delayed by an additional cycle to illustrate the phase transition.

Amplitude

The most prominent feature of the amplitude data is that the response at 14–18 Hz in the normal (Fig. 6b) and at 13–16 Hz in the achromat (Fig. 7b) falls to a minimum at the null intensity. The minimum in the ERG amplitude, like the corresponding perceptual null, is centered at ~0.2 $\log_{10}$ scot. td in the normal and at ~0.5 $\log_{10}$ scot. td in the achromat (see also Stockman et al., 1991). In both observers these minima coincide with the large changes in phase seen in Fig. 6a or 7a.

A model of the two rod signals

Although the phase and amplitude data are in general accord with the simple assumptions outlined in the Introduction, those assumptions fail to account for many critical aspects of the data. In particular, they allow no specific predictions about the dependence of the fast or the slow signal amplitudes on intensity, or about the dependence of the phase delay on intensity (except

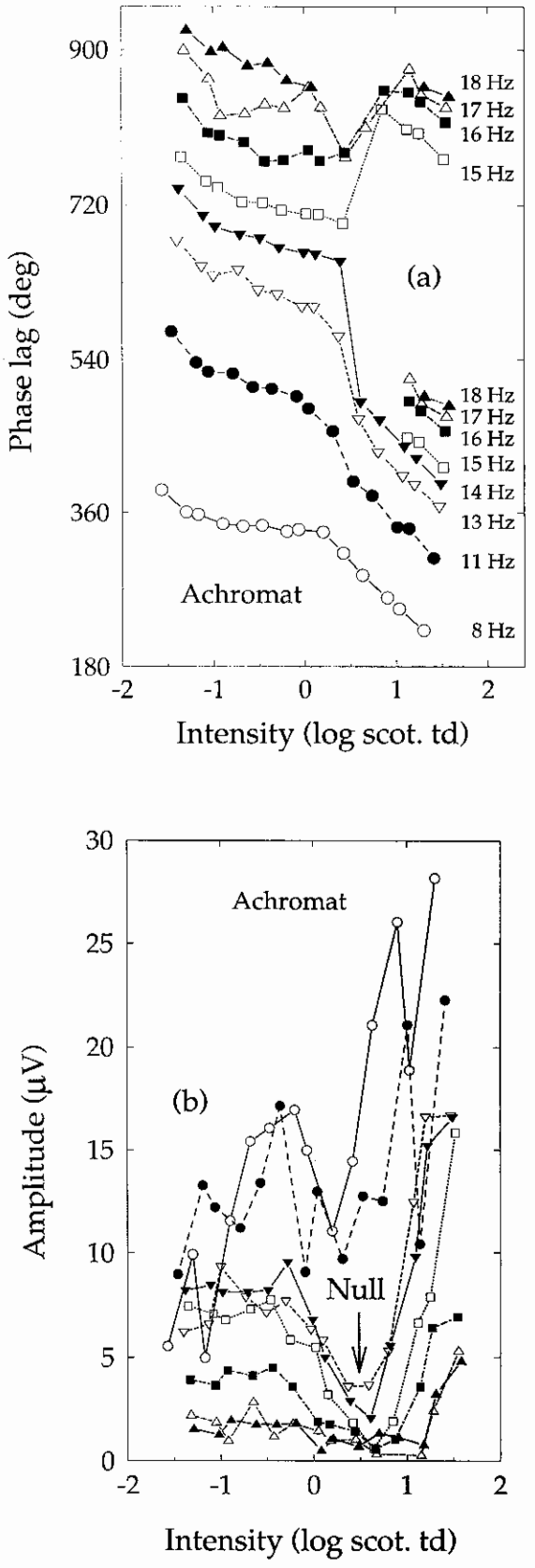

Fig. 7. The phase (a) and amplitude (b) of the ERG response for the achromat observer. Details are as for Fig. 6, except that in panel (a) the phase lags at 15–18 Hz are plotted twice, and in panel (b) there is no scale change along the amplitude axis.

at the null frequency). To correct this shortcoming, we have developed a model using the amplitude and phase data obtained from the ERG measurements. Our primary goal was to produce a model that depends upon a small number of straightforward assumptions, rather than to produce a model with enough parameters to meet some best-fitting criterion. Most of the model parameters (see Tables 1 and 2 in the Appendix) were derived by an iterative process, in which one parameter was varied incrementally to optimize the fit between the model and the data, then a second parameter value was varied, and so on. Whenever possible, the final parameter values were determined by the use of a least-squares, best-fitting algorithm (the Marquardt-Levenberg algorithm implemented in *SigmaPlot*, Jandel Scientific, San Rafael, CA). In accord with Ockham's razor, the model is restricted to just two underlying rod flicker signals. Clearly, a model based on three or more signals would do a better job of describing the ERG results, but it is not obvious from our analysis or from other psychophysical and electrophysiological flicker data that the postulation of additional signals is justified.

In the following section, we outline each of the simplifying premises that have been incorporated into the model (for a fuller account, including equations, see the Appendix). A discussion of single-flash ERG data and ERG models and their relationship to the flicker ERG data and model is presented in the Discussion.

Premise #1: The output signal is the linear combination of the slow and the fast rod signals

We assume that the amplitude and phase of the resultant rod flicker signal is the linear combination of the slow and fast rod signals. This assumption enables us to use simple vector addition when combining the two signals (see Fig. 14 in the Appendix).

Premise #2: Until it saturates, the slow rod signal grows logarithmically with intensity

We assume that the slow rod signal predominates at low scotopic intensity levels. At those levels, we find a roughly linear growth of the ERG response with the *logarithm* of intensity (see Figs. 6b and 7b above, and Figs. 9 and 11, below). This assumption is consistent with some form of gain control influencing the amplitude of the slow signal. Without a gain control, but with response compression, we might have expected signal growth to be hyperbolic, as is the case with the ERG *b*-wave [see eqn. (4) in Appendix].

Premise #3: At high scotopic levels the slow rod signal saturates with intensity

As the intensity is increased, the rate at which the phase delay of the ERG response changes from that of the slow signal to that of the fast signal is surprisingly rapid, even at those frequencies at which we assume the effects of destructive interference to be small or absent. Given our assumption that the two rod signals behave independently (see Premise #1), which precludes non-linear interactions between the two signals, we must account for the abrupt phase change by assuming either (1) that fast signal grows rapidly in that region, or (2) that the slow signal declines rapidly. A rapid increase in the fast signal is not supported by the amplitude data, which suggest a gradual, linear growth. However, a rapid decrease of the slow signal is suggested by the 8 Hz results for the normal (Fig. 7a) and the achromat (Fig. 7b), which show a decline in response amplitude just above 0.0 $\log_{10}$ scot. td. (see also p. 1556 of Sharpe et al., 1989). We assume therefore that above a certain critical intensity, the slow signal begins to saturate and at higher flicker frequencies actually declines.

The decline in the slow signal is modeled by the assumption that the flicker signal originating at the input (where the flicker is at 100% modulation) is temporally filtered before reaching the saturating stage. The temporal filter transforms the input signal into two components: a steady signal and a flickering signal of less than 100% modulation. Passing this composite signal through a saturating nonlinearity can further reduce the modulation of the flickering component. The saturating nonlinearity is modeled by a hyperbolic function. The combination of Premises #2 and #3 results in the response–intensity curves shown in Fig. 15 in the Appendix.

Premise #4: The fast rod signal grows linearly with intensity

We assume that the fast rod signal predominates at high scotopic intensity levels. At these levels, we find a roughly linear growth of the ERG response with intensity until the responses begin to saturate at ~1.5 $\log_{10}$ scot. td.

Premise #5: There is a time delay between the slow and fast rod signals

Earlier psychophysical and electrophysiological results show that over the range of visible rod flicker frequencies (0–~20 Hz) the phase delays between the slow and fast rod signals are consistent with a time delay, since they are roughly linear with frequency (Sharpe et al., 1989; Stockman et al., 1991). Accordingly, we assume a simple time delay between the two rod signals. A variant of Premise #5, in which the fast signal is not only time advanced with respect to the slow signal but also inverted in sign, is considered in the Discussion (see also Fig. 13).

One consequence of the assumption of a simple time delay is that there should be no difference in the relative amplitudes of the two rod signals as a function of frequency (i.e., no difference in the shapes of their temporal frequency responses). Our data suggest that this is roughly the case (see Fig. 12, below).

It is perhaps more common to think of delays between visual signals as resulting from additional stages of temporal filtering (e.g. RC filters) in the pathway of the more sluggish signal. In contrast to a time delay, temporal filtering causes not only an increase in phase delay, but also a relative decrease in signal amplitude at higher frequencies. It is important to note, however, that temporal filtering can be indistinguishable from a time delay if the time constants of the filtering stages are sufficiently short and if the measurements are restricted to low frequencies (e.g. between 0–20 Hz as in rod vision).

Premise #6: The rod system is subject to a time delay that declines linearly with log intensity

A transition from a slow signal to a signal that is ~33–35 ms faster does not suffice to account for the phase data of Figs. 6a and 7a. First, there is a gradual reduction in phase delay with intensity at all frequencies, even at the null frequency at which only a step-like phase transition is expected. Second, the overall phase advance is too large (by a factor of ~2) to be produced by a change in delay of only 33–35 ms.

We have modeled the gradual reduction in phase delay by assuming that, in addition to the transition from a slow to a

fast rod signal, there is an intensity-dependent reduction in the phase delay of both signals *together* (presumably arising in stages of the rod processing stream that are common to both rod pathways, such as the rod photoreceptor itself). We find that the reduction in phase delay can be approximated by assuming that there is a reduction in time delay that is linear with log intensity. The change in time delay with intensity can be added to an absolute time delay [estimated for an arbitrary intensity of 0.0 $\log_{10}$ scot td; see eqns. (9) and (10) in Appendix] to determine the absolute phase delay of the rod system at any given intensity.

Model fits

In Figs. 8–11 the predictions of the model are compared with the phase and amplitude data for the normal (Figs. 8 and 9, respectively) and for the achromat (Figs. 10 and 11, respectively). Two fits are shown in each case: (1) fits based on the assumption of simple time delays for all phase delays, as outlined above (i.e. phase delays that vary linearly with frequency); and (2) fits in which no assumption was made about the relationship of phase delay to frequency (i.e. phase delays that are allowed to vary independently of frequency). Further details are given below.

Phase lags

Figs. 8 and 10 show the predicted phase delays. In each figure, the predictions of the model based on time delays are shown as dotted lines. The fits that can be achieved by allowing the phase delay to vary independently of frequency are shown by the continuous lines. The phase data, which were shown previously in Figs. 6a and 7a, are indicated by the symbols. Not surprisingly, given the substantial increase in the number of fitted parameters, allowing the phase delay to vary independently of frequency accounts for the data better than the time delay model, but the improvement in fit is relatively small. For the dotted lines, the root mean square (rms) fitting errors are 15.25 deg in the normal and 20.02 deg in the achromat, and for the continuous lines they are 9.85 deg in the normal and 11.58 deg in the achromat. Except at 8 and 11 Hz, both predictions provide a plausible account of normal's phase data. For the achromat, however, allowing the phase delay to vary independently of frequency provides a clearly superior fit not only at 8 and 11 Hz, but also at the highest frequencies. The possible significance of these discrepancies are considered in the Discussion (see also Fig. 13).

In the normal, the time delay model predicts a phase difference of 181.33 deg between the two rod signals at 15 Hz, whereas the best-fitting phase delay at the frequency is 175.49 deg (see Table 1). Although this is a relatively small difference in phase, for reasons discussed above, the time delay model produces an apparent increase in the phase delay across the null intensity, whereas the best-fitting phase delay function indicates a decrease in delay (see Fig. 8). To emphasize the difference, we have plotted the 15-Hz phase data above the null intensity twice, the upper group being delayed by an additional cycle relative to the lower group.

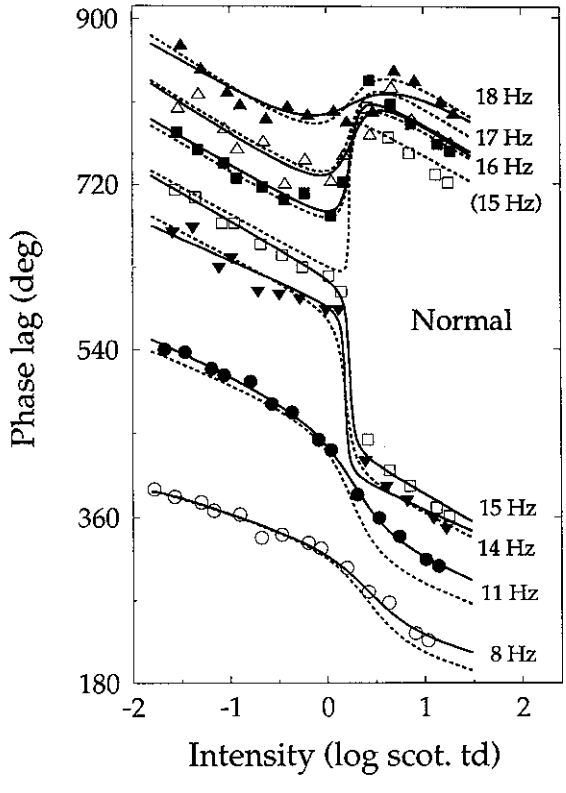

Fig. 8. The phase *vs.* intensity data of the normal observer fit by the predictions of the time delay model (dotted lines). The fit that can be obtained by allowing the phase delay to vary independently of frequency is shown by the solid lines. See text for details.

Amplitudes

In Fig. 9 for the normal and in Fig. 11 for the achromat, the predictions of the model are shown by the dotted lines. The fit that can be achieved by allowing the phase delay to vary independently of frequency is shown by the continuous lines (which often coincide with the dotted lines). In all panels, the amplitudes of the fast signal that were assumed for both fits are shown by the dotted-dashed lines and those of the slow signal are shown by the dashed lines. Again, allowing the phase delay to vary independently of frequency accounts for the data better than the time delay model at 11 Hz in the normal and the achromat, whereas the reverse is the case at 8 and 18 Hz in the normal and at 16–18 Hz in the achromat.

Overall, a linear growth with the logarithm of intensity provides a reasonably good description of the slow rod signal at low intensities; whereas a linear growth with intensity provides a good description of the fast signal. At intermediate intensities, the linear combination of the saturating slow signal and the fast signal provides a good, overall account of the change in the amplitude of the ERG signal.

Discussion

The ERG flicker recordings made in both the normal and the achromat observer add to the growing body of evidence supporting a duality in the processing of rod signals in the human visual system (Hecht et al., 1938; Conner & MacLeod, 1977; Conner, 1982; Sharpe et al., 1989; Stockman et al., 1991). The results demonstrate a transition between a slow and a fast rod signal at mesopic levels (i.e. levels at which both the rods and cones may be active in normal vision), which is manifested as a rapid change in phase and a minimum in the amplitude of the response near a frequency of 15 Hz.

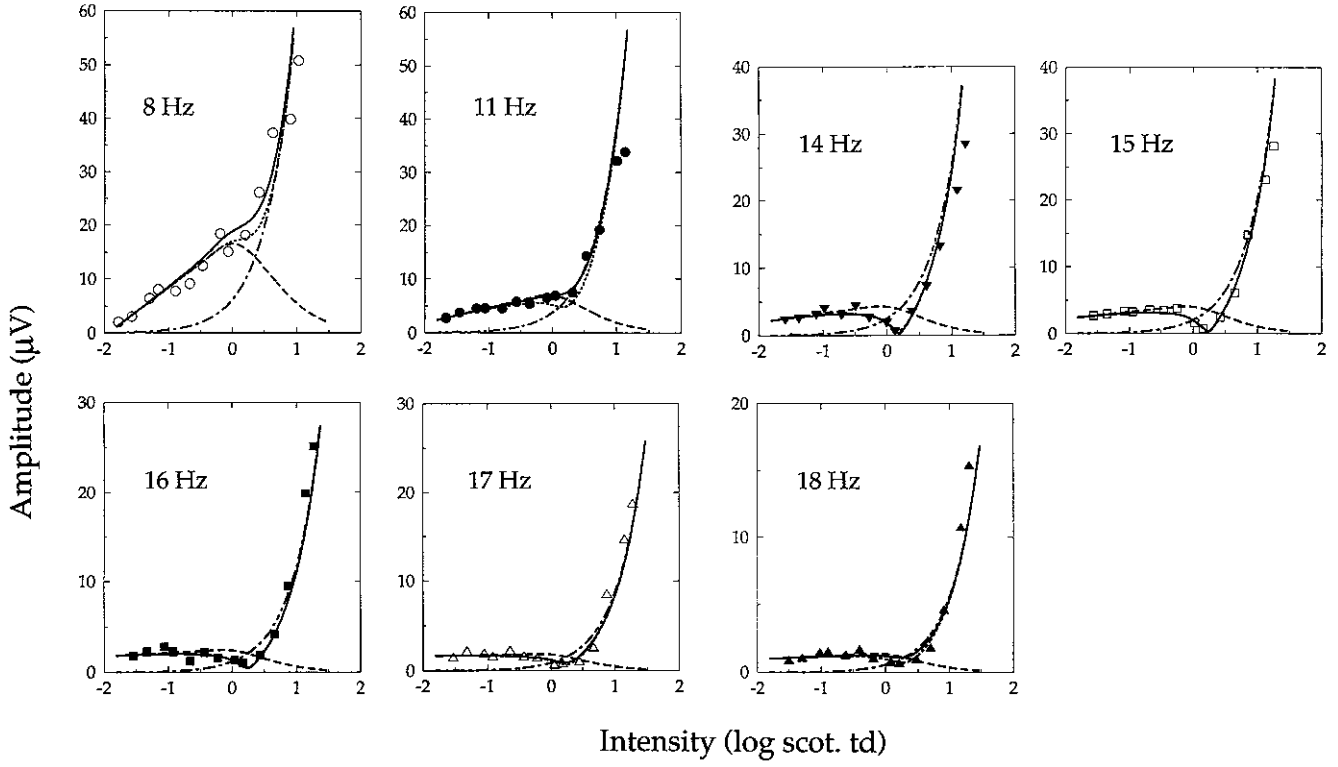

Fig. 9. The amplitude *vs.* intensity data of the normal observer (symbols) fit by the predictions of the time delay model (dotted lines). The fit that can be obtained by allowing the phase delay to vary independently of frequency is shown by the solid lines. The slow signal amplitudes (dashed lines) and fast signal amplitudes (dotted-dashed lines) assumed in the time delay model are also shown. (Note the changes in vertical scale with frequencies.) See text for details.

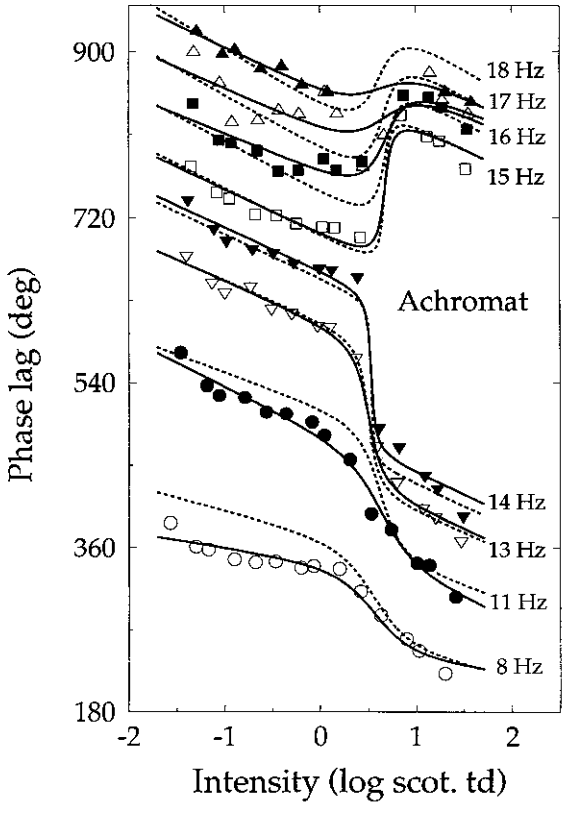

Fig. 10. Same as Fig. 8, except for the achromat observer.

We have modeled ERG data measured over more than 3 decades of intensity and over a range of frequencies from 8 to 21 Hz by a few simple premises. Although our model must inevitably be an oversimplification of a complex biological system, the final version accounts for the data surprisingly well. There are, however, several problems associated with the model and a number of possible refinements that can be applied to it, which we consider below.

The model

The temporal frequency responses of the slow and fast rod signals

Implicit in our model are assumptions about the temporal frequency responses of the slow and fast rod signals and how they depend on intensity. Fig. 12 shows the rod frequency response at three intensity levels: that of the assumed slow signal well below the null (filled circles) and just below the null (open circles); and that of the assumed fast signal above the null (open triangles).

A prominent feature of Fig. 12 is that the slow signal is larger in the achromat, whereas the fast signal is larger in the normal. The difference in the strengths of the fast rod signal between the two types of observer is explicable if the fast signal depends on rod–cone gap junctions and cone pathways, since those pathways are likely to be less developed in the achromat than in the normal (see Stockman et al., 1991, and below). The reason for the difference in the strengths of the slow rod signal is less clear, unless the slow and the fast rod signals mutually suppress each

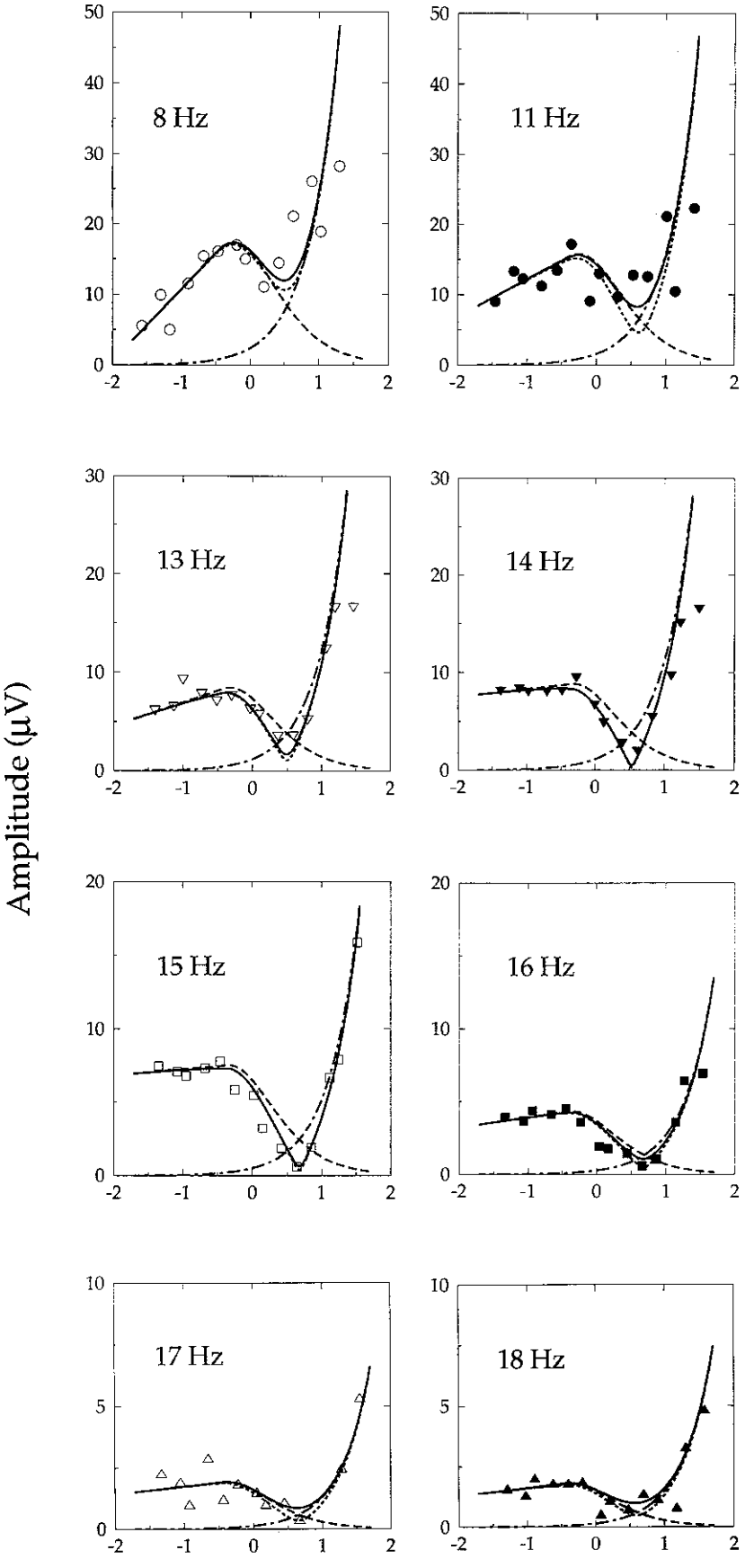

Fig. 11. Same as Fig. 9, except for the achromat observer.

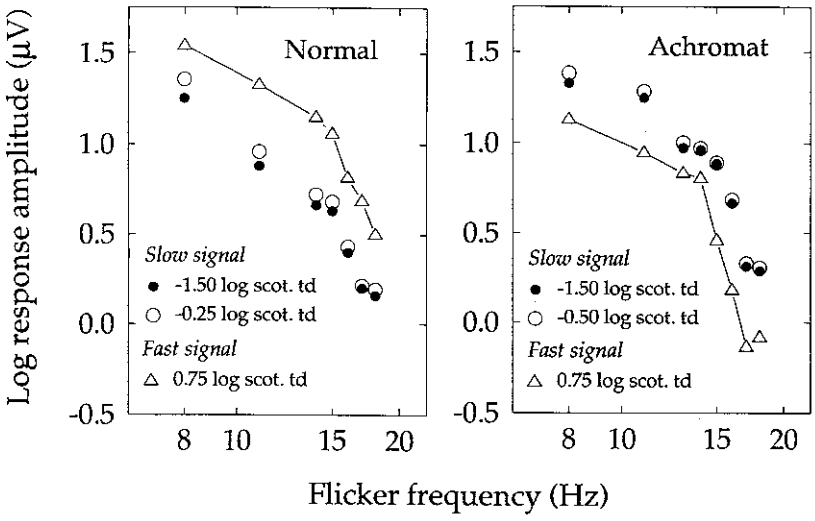

Fig. 12. The amplitude of the slow and fast rod signals predicted by the time delay model at three intensity levels for the normal observer (left) and achromat observer (right). See text for details.

other, so that a weakened fast signal leaves a stronger slow signal (see the following section).

The amplitude of the slow signal falls slightly more steeply with frequency at intensities just below the null than at those well below it. This steepening of the temporal frequency response with intensity is implied by the data (see Fig. 12), since the rate of increase in amplitude with log intensity is greater at low frequencies (see m in Tables 1 and 2). Though the effect is small, it is at odds with most measures of cone vision, which generally show a decrease in temporal integration with intensity, and a corresponding increase in the relative sensitivity to high frequencies (e.g. DeLange, 1958). Yet, in rod vision, most evidence suggests that there is little or no change in rod temporal integration in the intensity range up to ~0 log scot. td (see Sharpe et al., 1993, for a recent discussion).

It can also be seen in Fig. 12 that the fall-off of flicker amplitude with frequency is very similar for the fast and slow signals. This similarity is consistent with there being a time delay between the two signals, since such a delay should produce no change in the frequency response in going from the slow to the fast signal (but see above).

In accordance with the ERG data, we have assumed that the fast signal grows in proportion to intensity, and therefore that the shape of the temporal frequency response does not change with intensity. This result is inconsistent with comparable psychophysical measurements, which suggest that the frequency response of the fast signal falls less steeply with frequency (and becomes more bandpass) as the intensity is increased (Conner, 1982; Sharpe et al., 1989). The reason for the discrepancy between psychophysics and electrophysiology is unclear, but it could reflect changes in the temporal frequency response that are introduced after the generation of the ERG response, since such changes would selectively alter the psychophysical data. Suction electrode recordings of isolated rod outer segments, which show a slight speeding up of the time to peak of the rod response of <20% only at high mesopic intensities (Baylor et al., 1984; Hood & Birch, 1993; Kraft et al., 1993), are more consistent with the ERG data. It should be noted, of course, that the ERG is the sum of potentials from several sources, some of which may not directly affect the neural output from the retina. As such, discrepancies between electrophysiology and psychophysics should be expected.

At still higher intensities than those used in our experiments, the rod ERG response will saturate because the rod receptor response itself saturates (Baylor et al., 1984).

Nonlinear interactions between the slow and fast signal

A simplifying assumption of the model is that the slow and the fast rod signals are independent. A more complex model would be one in which the fast signal suppresses the slow signal (see Sharpe et al., 1989). Indeed, such suppression could give rise to the saturation of the slow signal that is required by the model (see Premise #3). However, a substantial problem with any model relying upon a nonlinear interaction between the two signals is that the (assumed) fast signal is only a small fraction of the slow signal when the slow signal first begins to saturate (see Figs. 9 and 11). Suppressive flicker interactions have been reported between rod and cone signals (e.g. Goldberg et al., 1983; Alexander & Fishman, 1984, 1985; Coletta & Adams, 1984; Arden & Hogg, 1985; Frumkes et al., 1986). It is an intriguing possibility that rod signals traveling through cone pathways might suppress rod signals traveling through rod pathways just as if they were cone signals.

Time delays

Fig. 13 shows the best-fitting time delays (continuous lines) or phase delays (symbols) for the normal (left panel) and achromat (right panel) observers. All values are tabulated in Tables 1 and 2 of the Appendix. The parameters are defined in equations in the Appendix.

The three lines in each panel represent the following: t_{abs} is the absolute time delay plotted as a function of frequency [t_{abs} is 117 ms for the normal and 130 ms for the achromat; it is defined as the time delay of the rod system at 0 $\log_{10}$ scot. td, see eqn. (10)]; t_{10} is the change in time delay per decade of intensity plotted as a function of frequency [t_{10} is 10.8 ms per decade for the normal and 9.6 ms for the achromat, see eqn. (9)]; and Δt is the time delay between the slow and the fast signals plotted as a function of frequency [Δt is 33.58 ms for the normal and 35.0 ms for the achromat, see eqn. (8a)]. The symbols represent the best-fitting phase delays when the phase delays were allowed to vary independently at each frequency. The error bars are ±2 asymptotic standard errors of the fitted parameters.

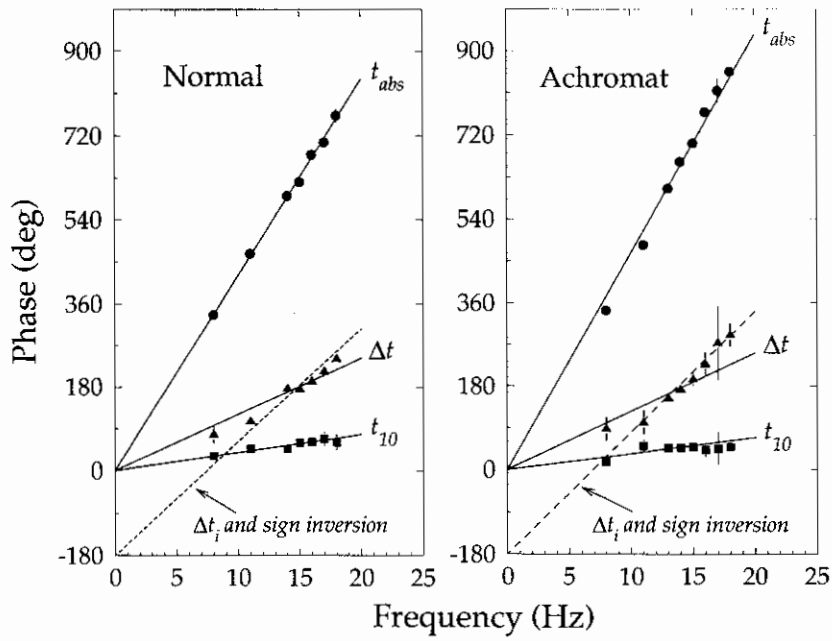

Fig. 13. Best-fitting phase delays determined independently at each frequency (symbols) compared with phase delays obtained by the assumption of simple time delays (lines) for the normal observer (left) and achromat observer (right). The error bars are ±2 asymptotic standard errors for the fitted parameters. See text for details.

The comparison between the best-fitting time delays (lines) and the best-fitting phase delays (symbols) provides some indication of the failures of the time delay model. The best-fitting phase delay could, in principle, take on any value. Nonetheless, the best-fitting values all lie fairly close to the straight lines t_{abs}, t_{10} and Δt; thus confirming, to a first approximation, that phase delays in the rod system (between 8 and 18 Hz) can be modeled by time delays. The agreement between the fitted phase delays (θ_{abs} in Tables 1 and 2) and the line t_{abs} (rms difference of 6.37 deg and 18.86 deg for the normal and achromat, respectively) and between the fitted phase delays (θ_{10} in Tables 1 and 2) and the line t_{10} (rms difference of 4.84 deg and 10.02 deg for the normal and achromat, respectively) is good. But that between the fitted phase delays ($\Delta\theta$ in Tables 1 and 2) and the line Δt (rms difference of 16.07 deg and 35.35 deg for the normal and achromat, respectively) is poor.

The deviations of $\Delta\theta$ from the Δt predictions are large at 8 and 11 Hz in both subjects, and at 17 and 18 Hz in the achromat (see Fig. 13). The fact that the deviations exhibited by the achromat are systematic suggests that the basic model may be incorrect. Indeed, a better fit to the data in the frequency range above 11 Hz is provided by a variant of the model, in which we assume that besides a time delay (Δt_i) between the two signals, there is an inversion of the sign of the fast signal relative to that of the slow signal (Fig. 13, dashed line labeled Δt_i *and sign inversion*). This produces a plot of phase delay vs. frequency that is also a straight line, but one which passes through −180 deg at 0 Hz rather than 0 deg [see eqn. (8b) in the Appendix]. The best-fitting time delays (Δt_i) with sign inversion are 67.39 ms for the normal and 72.44 ms for the achromat.

Though large, a delay of ~70 ms is not implausible. Comparable delays are typically reported between rod signals (from the slow pathway) and cone signals (e.g. Arden & Weale, 1954; Veringa & Roelofs, 1966; MacLeod, 1972; Sharpe et al., 1989). The required signal inversion could be produced in a single pathway by a nonlinear stage preceding a stage of rectification. One need only imagine a nonlinearity that is expansive at low signal amplitudes, linear at medium ones and compressive at high ones, and is followed by full-wave rectification. With this arrangement, the response at the fundamental frequency will reverse in phase and pass through an amplitude minimum as the nonlinearity changes from expansive to compressive.

To distinguish between the simple time delay and the simple time delay plus sign inversion variants of the model, we would require more data at frequencies closer to 0 Hz, where the predictions of the two differ by 180 deg. Other flicker ERG and psychophysical measurements (Sharpe et al., 1989; Stockman et al., 1991), as well as the 8-Hz ERG measurements shown above, suggest that the fast signal is not sign inverted. It is conceivable, however, that the fast signal is complex in origin: it may be composed of a sign-inverted signal at higher frequencies and a non-inverted signal at lower frequencies. Although the sign-inverted variant of the model might appear to support the corneally negative scotopic threshold response (STR) (Arden & Brown, 1965; Sieving et al., 1986; see below) as the source of the slow signal, it does not; for it is the fast signal, not the slow, that is sign inverted (through t_{abs} for the achromat could be extrapolated to −180 deg at 0 Hz).

It should be noted that it is the intercept of the phase lag *vs.* frequency function that defines the sign of the signal. Thus, the extrapolated functions for the slow signal and for the fast signal (labeled Δt) extrapolate to 0 deg at 0 Hz, which suggests that those signals are positive. In contrast, the function for the fast signal label Δt_i *and sign inversion* extrapolates to −180 deg at 0 Hz, which suggests that it is negative.

The flicker ERG, the single-flash ERG, and the two rod signals

To a first approximation, the flicker ERG results (and perceptual results) can be accounted for by just two components. Yet, over the same range of intensities, there are three main components in the ERG response to a single flash: the scotopic threshold response (STR), the DC component, and the *b*-wave (the last two are typically grouped together as the PII component).

It is clearly of interest to understand the relationship between the two flicker components and the three single-flash components, but the comparison is complicated because the two types of ERG are measured under very different conditions. The single-flash ERG is measured with flashes that are separated in time with the express purpose of avoiding the effects of light adaptation, whereas the flicker ERG is measured with prolonged trains of flashes. As a result, light adaptation plays a much greater role in the production of the flicker ERG response than of the single-flash ERG response. This problem is compounded by the observation that light adaptation can selectively spare one ERG component over another (Steinberg, 1969, Fig. 4).

Of the three single-flash components, the one with the highest sensitivity is the corneally negative STR, first identified and named by Sieving et al., 1986 (see also Arden & Brown, 1965; Schweitzer & Troelstra, 1965; Finkelstein et al., 1968). The DC component, in contrast to the STR, is a corneally positive response, which, along with the more transient *b*-wave, was originally defined as part of the PII process of the ERG (e.g. Granit, 1947). The distinctness of the DC component from the *b*-wave was made clear in cat first by Brown and Wiesel (1961*a*,*b*) and then by Steinberg (1969). The third main single-flash component, the *b*-wave, is a more transient response than either the DC potential or the STR. It is a corneally positive response that has a higher threshold than the DC component under most conditions (e.g. Brown & Wiesel, 1961), is more affected by light adaptation (Steinberg, 1969), and dominates the ERG at moderate to high intensities.

A clue to the relationship between the flicker and single-flash ERG is provided by the signs of the components. The DC component and the *b*-wave of the single-flash ERG are all corneally positive, whereas the STR is corneally negative. If we assume the basic model, in which both the slow and the fast components of the flicker ERG are positive (see above and Fig. 13), then we are led to the straightforward hypothesis that the slow rod signal corresponds to the DC component and the fast rod signal to the rod *b*-wave. However, if we assume the variant of the model, in which the fast signal is corneally negative and the slow signal corneally positive, there is no obvious correspondence.

Perhaps the most important evidence is provided by similarities between the response *vs.* intensity functions of the various components. The slow flicker ERG signal (see above), the STR (Sieving et al., 1986; Sieving & Nino, 1988), and the DC component (Schweitzer & Padmos, 1966; Steinberg, 1969; Knave et al., 1972) all grow linearly with the logarithm of intensity before they saturate. In contrast, the *b*-wave and the fast flicker ERG signal grow approximately linearly with intensity over the range of intensities used in these experiments. (The well-known concordance of the *b*-wave with the Naka-Rushton hyperbolic saturation function (Fulton & Rushton, 1978; Arden et al., 1983; Peachey et al., 1989) implies a roughly linear growth of the *b*-wave with intensity at levels well below the half-saturation constant.) These similarities imply that the slow flicker signal, the DC component, and the STR reflect activity in one common pathway, and the fast flicker signal and the *b*-wave activity in another. If this is the case, then for the rod-cone gap junction to be the origin of the fast rod signal, as we suggest below, we must suppose that the rod *b*-wave also originates in cone pathways. Although an interesting possibility, there is as yet little evidence to support this view. To the extent that rod–cone gap junctions facilitate the transmission of rod signals through cone pathways (see below), however, the rod *b*-wave must reflect activity in cone as well as in rod pathways.

Hood and Birch (1992) have proposed a computational model of the *b*-wave that comprises three stages of temporal filtering separated by two static nonlinearities. The change in the implicit time of the *b*-wave is assumed to result primarily from the saturation of the rod response at the first static nonlinearity. Their model predicts a change in the *b*-wave implicit time of ~40 ms per decade of intensity in the range from 0 to 1.5 log scot. td-s (see their Fig. 10). This decline is substantially more than the change in delay suggested by the rod flicker ERG results, which average ~10 ms per decade (see Tables 1 and 2). Our model does produce changes of this magnitude, of course, but only due to the transition from the slow signal to the fast signal. Perhaps, then, Hood and Birch's *b*-wave data provide evidence for a transition from a slow to a fast rod signal in the single-flash ERG. Indeed, for brief flashes, the intensity region, 0 to 1.5 log scot. td-s is where one might expect it.

One exception to the use of isolated single flashes to determine the ERG is Fulton and Rushton (1978), who measured the *a*-wave and *b*-wave on a series of background fields of increasing intensity. Their *b*-wave results (see their Fig. 3b) are consistent with a gain control operating at low intensities followed by saturation at higher intensities—much like our model of the slow rod signal.

Two rod signals, two rod pathways?

As outlined above, evidence mainly from the cat and the rabbit indicates that there are two main pathways by which rod signals can travel through the mammalian retina from the rods to the ganglion cells (see, for example, Kolb & Nelson, 1983; Sterling et al., 1986; Daw et al., 1990; Wässle & Boycott, 1991). The main pathway is from rods to rod bipolars, to AII amacrine cells, and then to either ON cone bipolars and ON ganglion cells or to OFF ganglion cells. The secondary pathway is by way of gap junctions between the rods and cones, through which rod signals have access to cone bipolars and thence to ON and OFF ganglion cells.

The idea that the slow and fast rod signals revealed in the human ERG and in human perceptual observations are electrophysiological and perceptual correlates of these two mammalian pathways is certainly an appealing one. Indeed, there are several features of our results that support this idea. For example, the linear growth of the fast rod signal with increasing intensity suggests that it bypasses the usual postreceptoral, rod gain control, which according to our model causes a saturation at low mesopic levels. If the main gain control is located in the rod–rod bipolar-amacrine II cell pathway, then rod–cone gap junctions could provide the route by which the fast rod signal is able to avoid it. Moreover, calculations by Smith et al. (1986) suggest that the rod–cone gap junction pathway should become important in the mammalian retina at the levels at which the fast rod signal becomes prominent in our human measurements.

Unfortunately, there have been few attempts to find direct correlates between the two rod signals identified in humans and mammalian recordings. An exception is Nelson et al. (1993), who reported phase delays between 10.5 or 11.3 Hz flicker signals in the AII cells and the OFF alpha ganglion cells that are consistent with the delays between the two rod signals in humans (see their Fig. 9, right). Importantly, they also found that the AII response saturates at a relatively low intensity, which is con-

sistent with our model of the slow signal. And, more recently, Schneeweis and Schnapf (1995) have directly recorded rod signals in primate cones, thus establishing in primates that rod signals can travel through cones to ON and OFF cone bipolars.

Nevertheless, there is a problem in supposing that the rod–cone gap junction is the substrate of the fast rod signal. It is the evidence presented here and in our previous paper (Stockman et al., 1991) that demonstrates a fast rod signal in an achromat observer who lacks functioning cones. With one exception (Larsen, 1921), histological studies of the retinas of totally color blind observers (with reduced visual acuity) have reported cone numbers in the totally color blind eye to be vastly fewer than those found in the normal retina, and the cones themselves are often deformed near the fovea (Harrison et al., 1960; Falls et al., 1965; Glickstein & Heath, 1975). Although these studies might be taken as evidence against the rod–cone gap junction as the origin of the fast rod signal, the inner segments of the few non-functioning cones in the totally color blind observers may still provide a viable pathway for the fast rod signal *via* rod–cone gap junctions, even though the outer segments produce no cone signal. The fact that the inner nuclear layer and ganglion cell layer are normal in these observers (Glickstein & Heath, 1975) suggests that their cone pathways are receiving rod initiated innervation *via* the rod–cone gap junctions (a possibility suggested to us by Robert G. Smith). The emergence of the fast rod signal at a higher intensity in our achromat observer than in all normal observers measured so far (Sharpe et al., 1989, 1993, 1994) is consistent with the dependence of the fast rod signal on a vestigial cone pathway in the achromat.

Other possible substrates of the two rod signals

Although we hold that the anatomical substrates of the slow and fast rod signals are most likely to be, respectively, the rod-to-rod bipolar pathway, and the rod-to-cone-to-cone bipolar pathway *via* rod–cone gap junctions, other substrates are possible. In deciding between them, it is important to consider evidence that might indicate where the two signals first arise and where they subsequently recombine and cancel.

The ERG data suggest that the slow and fast rod signals arise at or before the bipolar cell level. For if the two signals arose at a more proximal site, they would not be evident in ERG components that originate primarily in distal retina, such as the DC potential or the *b*-wave (see, for example, Tomita, 1950; Brown & Wiesel, 1961*b*; Arden & Brown, 1965; Miller & Dowling, 1970; Sieving et al., 1986).

The site at which the slow and fast flicker signals recombine is less clear. One possibility is that the signals recombine and cancel at or before the bipolar cells (i.e. at or before the generation of the distal ERG components), in which case the null in the ERG and the null in perception must occur together, as we find. Alternatively, the neural recombination of two rod signals could be proximal to the generation of the ERG, with the null in the ERG being found only in the electrically averaged response of the retina as a whole, but not in the response of any individual neural cell. In this case, the neural cancellation that gives rise to the perceptual null and the electrical cancellation that gives rise to the ERG null need not occur at the same intensity.

The hypothesis that the fast rod signal derives from rod–cone gap junctions satisfies the requirement that the two rod signals arise at or before the bipolar cells. Yet, it implies different sites of neural and electrical cancellation, since rod and cone pathways converge after the rod bipolar cells, either at the electrical gap junctions between the AII amacrine cells and the ON cone bipolar cells or at the chemical synapses between the AII amacrine cells and the OFF ganglion cells. To be consistent with our results, which show a concurrence of the electrophysiological and psychophysical nulls, the more distal electrical cancellation must occur at the same intensity as the more proximal neural cancellation. While such a coincidence is conceivable, it would be inescapable if the two rod signals recombined at or before the cells that generate the ERG response. There are several ways by which this could occur.

One way would be if the two rod signals originate from different populations of rod photoreceptors with distinct response properties. However, there seems to be no evidence for such a duality in mammals, with the exception perhaps of the ground squirrel (Jacobs, 1990). The variability that is found in suction electrode recordings from the outer segments of individual primate and human rods is too small and too continuous to support such a duality (Baylor et al., 1984; Tamura et al., 1991). Alternatively, an early nulling site might occur if the faster signal depended on rod–rod gap junctions, which have been shown to produce networks that speed up the rod response in toads (Detwiler et al., 1978). Rod–rod gap junctions, however, have not been found in primates (Raviola & Gilula, 1973, 1975). Lastly, an early nulling site might occur if one of the rod signals depended on horizontal cells, and the other on more direct connections. Yet, we demonstrate elsewhere that the two rod signals integrate over similar spatial extents for fields greater than 1 deg. This argues against the selective role of far-ranging horizontal cells in the production of one or other of the rod signals (Sharpe et al., 1994). Thus, hypotheses of the origin of the two rod pathways, other than the rod–cone gap junction one, seem to have little support (see Sharpe & Stockman, submitted, for a more detailed discussion).

Conclusion

We have presented new evidence for a duality of rod signal transmission in gross, ERG recordings from the human eye, which complement and confirm previous phenomenological and psychophysical observations. The correlation between psychophysical and electrophysiological observations is important, because it establishes that the two signals have a definite significance for the visual system and flicker perception. Although histological observations in rat, cat, and rabbit have revealed the presence of two anatomical pathways for the transmission of rod signals, the relevancy of these pathways will remain uncertain and speculative until their function has been confirmed by electrophysiological and behavioral or psychophysical observations. In our model of the rod duality, we provide predictions of the way in which the amplitude and phase of the slow and the fast rod signal depend on intensity. With this information, the two signals should be easily revealed in micro-electrode recordings of mammalian retina. It would be very pleasing if the two rod pathways first revealed by psychophysical measurements, and now confirmed by electrophysiological recordings in man, turn out to be correlates of the two rod pathways recently revealed by anatomical and physiological observations in lower mammals. Yet, for the several reasons outlined above, such a correspondence is by no means certain.

Acknowledgments

We thank S. E. Apitz, L. J. Frishman, D. C. Hood, W. Makous, D. I. A. MacLeod, and R. Nelson for advice and comments. We are especially grateful to R. G. Smith for several helpful discussions. Supported by NSF Grant IBN 92-10046, by NIH Grant EY 10206, by DFG (Bonn) Grants RU 457/1-2 and SFB 325 (B13), and by the Heisenberg-Programme.

References

Alexander, K.R. & Fishman, G.A. (1984). Rod-cone interaction in flicker perimetry. *British Journal of Ophthalmology* **68**, 303–309.

Alexander, K.R. & Fishman, G.A. (1985). Rod-cone interaction in flicker perimetry: Evidence for a distal retinal locus. *Documenta Ophthalmologica* **60**, 3–36.

Alpern, M., Falls, H.F. & Lee, G.B. (1960). The enigma of typical total monochromacy. *American Journal of Ophthalmology* **50**, 996–1012.

Arden, G.B. & Brown, K.T. (1965). Some properties of components of the cat electroretinogram revealed by local recordings under oil. *Journal of Physiology* (London) **176**, 429–461.

Arden, G.B., Carter, R.M., Hogg, C.R., Powell, D.J., Ernst, W.J.K., Clover, G.M., Lyness, A.L. & Quinlan, M.P. (1983). A modified ERG technique and the results obtained in X-linked retinitis pigmentosa. *British Journal of Ophthalmology* **67**, 419–430.

Arden, G.B. & Hogg, C.R. (1985). Rod-cone interaction and analysis of retinal disease. *British Journal of Ophthalmology* **69**, 404–415.

Arden, G.B. & Weale, R.A. (1954). Variations of the latent period of vision. *Proceedings of the Royal Society* (London) **B142**, 258–269.

Baylor, D.A., Nunn, B.J. & Schnapf, J.L. (1984). The photocurrent, noise and spectral sensitivity of rods of the monkey *Macaca fascicularis*. *Journal of Physiology* (London) **357**, 575–607.

Blakemore, C.B. & Rushton, W.A.H. (1965). Dark adaptation and increment threshold in a rod monochromat. *Journal of Physiology* (London) **181**, 612–628.

Brown, K.T. & Wiesel, T.N. (1961*a*). Analysis of the intraretinal electroretinogram in the intact cat eye. *Journal of Physiology* (London) **158**, 229–256.

Brown, K.T. & Wiesel, T.N. (1961*b*). Localization of origins of electroretinogram components by intraretinal recording in the intact cat eye. *Journal of Physiology* (London) **158**, 257–280.

Chun, M.-H., Han, S.-H., Chung, J.-W. & Wässle, H. (1993). Electron microscopic analysis of the rod pathway of the rat retina. *Journal of Comparative Neurology* **332**, 421–432.

Coletta, N.J. & Adams, A.J. (1984). Rod-cone interaction in flicker detection. *Vision Research* **24**, 1333–1340.

Conner, J.D. (1982). The temporal properties of rod vision. *Journal of Physiology* (London) **332**, 139–155.

Conner, J.D. & MacLeod, D.I.A. (1977). Rod photoreceptors detect rapid flicker. *Science* **195**, 689–699.

Dacheux, R.F. & Raviola, E. (1986). The rod pathway in the rabbit retina: a depolarizing bipolar and amacrine cell. *Journal of Neuroscience* **6**, 331–345.

Daw, N.W., Jensen, R.J. & Brunken, W.J. (1990). Rod pathways in mammalian retinae. *Trends in Neurosciences* **13**, 110–115.

De Lange, H. (1958). Research into the dynamic nature of the human fovea-cortex systems with intermittent and modulated light. I. Attenuation characteristics with white and colored light. *Journal of the Optical Society of America* **48**, 777–784.

Detwiler, P.B., Hodgkin, A.L. & McNaughton, P.A. (1978). A surprising property of electrical spread in the network of rods in the turtle retina. *Nature* **274**, 562–565.

Dodt, E. & Walther, J.B. (1958). Der photopische Dominator im Flimmer-ERG der Katze. *Pflügers Archiv für die gesamte Physiologie des Menschen und Tiere* **266**, 175–186.

Falls, H.F., Wolter, J.R. & Alpern, M. (1965). Typical total monochromacy. *Archives of Ophthalmology* **74**, 610–616.

Famiglietti, E.V. & Kolb, H. (1975). A bistratified amacrine cell and synaptic circuitry in the inner plexiform layer of the retina. *Brain Research* **84**, 293–300.

Finkelstein, D., Gouras, P. & Hoff, M. (1968). Human electroretinogram near the absolute threshold of vision. *Investigative Ophthalmology and Visual Science* **7**, 214–218.

Frumkes, T.E., Naarendorp, F. & Goldberg, S.H. (1986). The influence of cone adaptation upon rod mediated flicker. *Vision Research* **26**, 1167–1176.

Fulton, A.B. & Rushton, W.A.H. (1978). The human rod ERG: correlation with psychophysical response in light and dark adaptation. *Vision Research* **18**, 793–800.

Glickstein, M. & Heath, G.G. (1975). Receptors in the monochromat eye. *Vision Research* **15**, 633–636.

Goldberg, S.H., Frumkes, T.E. & Nygaard, R.W. (1983). Inhibitory influence of unstimulated rods in the human retina: Evidence provided by examining cone flicker. *Science* **221**, 180–182.

Granit, R. (1947). *Sensory Mechanisms of the Retina*. London: Oxford University Press.

Harrison, D., Hoefnagel, D. & Hayward, J.N. (1960). Congenital total colour blindness, a clinicopathological report. *Archives of Ophthalmology* **64**, 685–692.

Hecht, S., Shlaer, S., Smith, E.L., Haig, C. & Peskin, J.C. (1938). The visual functions of a completely color blind person. *American Journal of Physiology* **123**, 94–95.

Hecht, S., Shlaer, S., Smith, E.L., Haig, C. & Peskin, J.C. (1948). The visual functions of the complete color-blind. *Journal of General Physiology* **31**, 459–472.

Hess, R.F. & Nordby, K. (1986). Spatial and temporal limits of vision in the achromat. *Journal of Physiology* (London) **371**, 365–385.

Hood, D.C. & Birch, D.G. (1992). A computational model of the amplitude and implicit time of the *b*-wave of the human ERG. *Visual Neuroscience* **8**, 107–126.

Hood, D.C. & Birch, D.G. (1993). Light adaptation of the human rod receptors: the leading edge of the human *a*-wave and models of rod receptor activity. *Vision Research* **33**, 1605–1618.

Jacobs, G.H. (1990). Duplicity theory and ground squirrels: linkages between photoreceptors and visual function. *Visual Neuroscience* **5**, 311–318.

Knave, B., Moller, A. & Persson, H.E. (1972). A component analysis of the electroretinogram. *Vision Research* **12**, 1669–1684.

Kolb, H. (1977). The organization of the outer plexiform layer in the retina of the cat: Electron microscopic observations. *Journal of Neurocytology* **6**, 131–153.

Kolb, H. (1979). The inner plexiform layer in the retina of the cat: Electron microscopic observations. *Journal of Neurocytology* **8**, 295–329.

Kolb, H. & Famiglietti, E.V. (1974). Rod and cone pathways in the inner plexiform layer of the cat retina. *Science* **186**, 47–49.

Kolb, H. & Nelson, R. (1983). Rod pathways in the retina of the cat. *Vision Research* **23**, 301–302.

Kolb, H. & Nelson, R. (1984). Neural architecture of the cat retina. In *Progress in retinal research*, ed. Osborne, N. & Chader, G., pp. 21–60. New York: Pergamon Press.

Kraft, T.W., Schneeweis, D.M. & Schnapf, J.L. (1993). Visual transduction in human rod photoreceptors. *Journal of Physiology* (London) **464**, 747–765.

Larsen, H. (1921). Präparate von einem monochromatischen Auge. *Klinische Monatsblätter für Augenheilkunde* **67**, 301–302.

MacLeod, D.I.A. (1972). Rods cancel cones in flicker. *Nature* **235**, 173–174.

Marmor, M.F., Arden, G.B., Nilsson, S.E.G. & Zrenner, E. (1989). Standard for clinical electroretinography. *Archives of Ophthalmology* **107**, 816–819.

Miller, R.F. & Dowling, J.E. (1970). Intracellular responses of the Müller (glial) cells of mudpuppy retina: Their relation to the b-wave of the electroretinogram. *Journal of Neurophysiology* **33**, 323–341.

Müller, F., Wässle, H. & Voight, T. (1988). Pharmacological modulation of the rod pathway in cat retina. *Journal of Neurophysiology* **59**, 1657–1672.

Nelson, R. (1977). Cat cones have rod input: a comparison of the response properties of cones and horizontal cell bodies in the retina of the cat. *Journal of Comparative Neurology* **172**, 109–136.

Nelson, R. (1982). AII amacrine cells quicken time course of rod signals in the cat retina. *Journal of Neurophysiology* **47**, 928–947.

Nelson, R. & Kolb, H. (1983). Synaptic patterns and response properties of bipolar and ganglion cells in the cat retina. *Vision Research* **23**, 1183–1195.

Nelson, R., Kolb, H. & Freed, M.A. (1993). OFF-alpha and OFF-beta ganglion cells in the cat retina. I: Intracellular electrophysiology and HRP stains. *Journal of Comparative Neurology* **329**, 68–84.

NORDBY, K.N. & SHARPE, L.T. (1988). The directional sensitivity of the photoreceptors in the human achromat. *Journal of Physiology* (London) **399**, 267–281.

PEACHEY, N.S., ALEXANDER, K.R., DERLACKI, D.J. & FISHMAN, G.A. (1992). Light adaptation, rods, and the human cone flicker ERG. *Visual Neuroscience* **8**, 145–150.

PEACHEY, N.S., ALEXANDER, K.R. & FISHMAN, G.A. (1989). The luminance-response function of the dark-adapted human electroretinogram. *Vision Research* **29**, 263–270.

RAVIOLA, E. & GILULA, N.B. (1973). Gap junctions between photoreceptor cells in the vertebrate retina. *Proceedings of the National Academy of Sciences of the U.S.A.* **70**, 1677–1681.

RAVIOLA, E. & GILULA, N.B. (1975). Intramembrane organization of specialized contacts in the outer plexiform layer of the retina. *Journal of Cell Biology* **65**, 192–222.

SCHNEEWEIS, D.M. & SCHNAPF, J.L. (1995). Photovoltage of rods and cones in the macaque retina. *Science* **268**, 1053–1056.

SCHWEITZER, N.M.J. & PADMOS, P. (1966). The microstructure of the human scotopic ERG. In *The clinical value of electroretinography, ISCERG Symposium*, ed. GHENT, Institute for Perception pp. 198–204. Basel: Karger.

SCHWEITZER, N.M.J. & TROELSTA, A. (1965). A negative component in the b-wave of the human ERG. *Ophthalmologica* **149**, 230–235.

SHARPE, L.T., COLLEWIJN, H. & NORDBY, K. (1986). Fixation, pursuit and nystagmus in a complete achromat. *Clinical Vision Sciences* **1**, 39–49.

SHARPE, L.T., FACH, C.C. & STOCKMAN, A. (1993). The spectral properties of the two rod pathways. *Vision Research* **33**, 2705–2720.

SHARPE, L.T., HOFMEISTER, J., FACH, C.C. & STOCKMAN, A. (1994). Spatial relations of flicker signals in the two rod pathways. *Journal of Physiology* (London) **474**, 421–431.

SHARPE, L.T. & NORDBY, K. (1990). The photoreceptors in the achromat. In *Night Vision: basic, clinical and applied aspects*, ed. HESS, R., SHARPE, L.T. & NORDBY, K., pp. 335–389. Cambridge: Cambridge University Press.

SHARPE, L.T. & STOCKMAN, A. (submitted). Two rod pathways: The importance of seeing nothing.

SHARPE, L.T., STOCKMAN, A., FACH, C.C. & MARKSTAHLER, U. (1993). Temporal and spatial summation in the human rod visual system. *Journal of Physiology* (London) **463**, 325–348.

SHARPE, L.T., STOCKMAN, A. & MACLEOD, D.I.A. (1989). Rod flicker perception: Scotopic duality, phase lags and destructive interference. *Vision Research* **29**, 1539–1559.

SIEVING, P.A., FRISHMAN, L.J. & STEINBERG, R.H. (1986). Scotopic threshold response of proximal retina of cat. *Journal of Neurophysiology* **56**, 1049–1061.

SIEVING, P.A. & NINO, C. (1988). Scotopic threshold response (STR) of the human electroretinogram. *Investigative Ophthalmology and Visual Science* **29**, 1608–1614.

SMITH, R.G., FREED, M.A. & STERLING, P. (1986). Microcircuitry of the dark-adapted cat retina: Functional architecture of the rod-cone network. *Journal of Neuroscience* **6**, 3505–3517.

STEINBERG, R.H. (1969). Comparison of the intraretinal b-wave and d.c. component in the *area centralis* of cat retina. *Vision Research* **9**, 317–331.

STERLING, P., FREED, M. & SMITH, R.G. (1986). Microcircuitry and functional architecture of the cat retina. *Trends in Neurosciences* **9**, 186–192.

STERLING, P., FREED, M. & SMITH, R.G. (1988). Architecture of rod and cone circuits to the *on*-beta ganglion cells. *Journal of Neuroscience* **8**, 623–642.

STOCKMAN, A., SHARPE, L.T., ZRENNER, E. & NORDBY, K. (1991). Slow and fast pathways in the human rod visual system: ERG and psychophysics. *Journal of the Optical Society of America A* **8**, 1657–1665.

TAMURA, T., NAKATANI, K. & YAU, K.-W. (1991). Calcium feedback and sensitivity in primate rods. *Journal of General Physiology* **98**, 95–130.

TOMITA, T. (1950). Studies on intraretinal action potential Part I. Relation between the localization of micro-pipette in the retina and the shape of the intraretinal action potential. *Journal of Neurophysiology* **1**, 110–117.

VERINGA, F. & ROELOFS, J. (1966). Electro-optical stimulation in the human retina. *Nature* **211**, 321–322.

WÄSSLE, H. & BOYCOTT, B.B. (1991). Functional architecture of the mammalian retina. *Physiological Reviews* **71**, 447–480.

WILLIAMS, T.P. & GALE, J.G. (1977). A critique of an incremental threshold function. *Vision Research* **17**, 881–882.

WYSZECKI, G. & STILES, W.S. (1982). *Color Science* (2nd ed.). New York: Wiley.

Appendix: The model

Premise #1: The output signal is the linear combination of the slow and the fast rod signals

This premise is illustrated in Fig. 14 in the form of a vector diagram.

The vector equation for predicting the phase advance (β) of the combined slow and fast rod signals, relative to the phase lag of the slow signal, is

$$\beta = \tan^{-1}\left[\frac{r \sin \Delta\theta}{1 + r \cos \Delta\theta}\right] \quad (1)$$

where $\Delta\theta$ is the phase difference between the slow and the fast rod signals (see Premise #5) and r is the ratio of the fast signal response magnitude, R_f (see Premise #4), to the slow signal response magnitude, R_s (see Premises #2 and 3). (In all equations, phase angle is in degrees, time in milliseconds, response amplitude in microvolts, and intensity in scot. td.)

The vector equation for predicting the magnitude of the resultant rod flicker signal (R_{s+f}) is

$$R_{s+f} = \sqrt{R_s^2 + R_f^2 - 2R_sR_f \cos(180 - \Delta\theta)} \quad (2)$$

Premise #2: Until it saturates, the slow rod signal (R_s) grows logarithmically with intensity

The response–intensity function of the slow rod signal at lower intensities is modeled by the equation:

$$R_s = m \log I + c \quad (3)$$

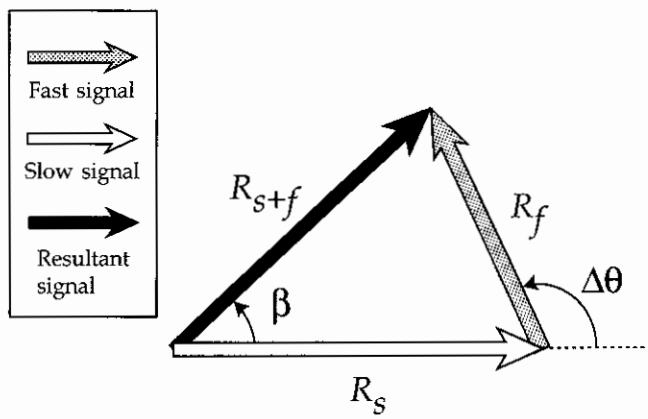

Fig. 14. Model for predicting the amplitude (R_{s+f}) and phase advance (β) of the resultant rod flicker signal (black arrow) from the linear vector sum of the slow rod signal (white arrow) and the fast rod signal (stippled arrow). R_s is the slow signal response magnitude; R_f, the fast signal response magnitude; and $\Delta\theta$ is the phase difference between the slow and fast rod signals.

Table 1. *Model parameters for the normal*

	Frequency						
	8	11	14	15	16	17	18
Slow signal							
Slope, m (μV per log scot. td)	9.08	2.80	1.26	1.01	0.37	0.11	0.23
Intercept, c (μV)	17.55	7.50	4.57	4.25	2.51	1.85	1.43
R_{max} (μV)	96.15	96.15	96.15	96.15	96.15	96.15	96.15
σ (scot. td)	0.70	0.70	0.70	0.70	0.70	0.70	0.70
Modulation, x	0.500	0.254	0.166	0.156	0.097	0.074	0.056
Fast signal							
Scaling constant, k	6.191	3.790	2.517	2.042	1.166	0.867	0.564
Slow *vs.* fast phase lag (deg)							
α (fitted)	77.38	106.27	176.77	175.49	192.91	213.89	241.23
α (Δt = 33.58 ms)	96.71	132.98	169.24	181.33	193.42	205.51	217.60
Phase change per decade (deg per log scot. td)							
ϕ (fitted)	31.28	47.10	46.81	60.41	62.08	68.63	61.18
ϕ (t_{10} = 10.79 ms per log scot. td)	31.07	42.72	54.38	58.27	62.15	66.03	69.91
Absolute phase delay (deg)							
ω (fitted)	336.12	467.31	591.10	620.38	678.83	705.73	762.11
ω (t_{abs} = 116.62 ms)	335.87	461.82	587.76	629.75	671.73	713.71	755.70

where m is the slope and c is the intercept (i.e. the value of R_s at $\log I = 0$). The values of m and c given in Tables 1 and 2 are best-fitting values.

Premise #3: At high scotopic levels the slow rod signal (R_s) saturates with intensity

The rate at which the phase delay of the ERG response changes from the phase of the slow signal to that of the fast signal depends on (1) the phase difference between the two rod signals ($\Delta\theta$) and (2) the change in the ratio of the fast to slow signal sizes (R_f/R_s or r) with intensity [see eqn. (1)]. At frequencies near the null frequency, when $\Delta\theta$ is close to 180 deg, an abrupt step-like phase change of ~180 deg will occur when $r = 1$, whatever the rate of growth of r (see Fig. 3d). At other frequencies, when $\Delta\theta$ is closer to 90 deg or 270 deg, the phase change depends more critically on the rate of growth of r with intensity: a rapid phase change implies a rapid increase in r. It can be seen in Figs. 6a and 7a that there is a rapid phase change in the region of the null *at all frequencies*—not just at frequencies near the null frequency. To produce such a rapid change at all frequencies, we assume that there is an abrupt increase in r in the region of the null that results from a saturation of the slow signal.

To model a saturation of the slow signal, we have used a modified version of the following hyperbolic saturation function:

$$R = \frac{IR_{\max}}{(I + \sigma)} \tag{4}$$

Table 2. *Model parameters for the achromat*

	Frequency							
	8	11	13	14	15	16	17	18
Slow signal								
Slope, m (μV per log scot. td)	10.26	5.33	2.37	0.79	0.40	0.70	0.31	0.32
Intercept, c (μV)	21.00	17.53	9.32	9.11	7.66	4.62	2.05	1.93
R_{max} (μV)	100.30	100.30	100.30	100.30	100.30	100.30	100.30	100.30
σ (scot. td)	0.40	0.40	0.40	0.40	0.40	0.40	0.40	0.40
Modulation, x	0.500	0.470	0.286	0.298	0.260	0.159	0.074	0.069
Fast signal								
Scaling constant, k	2.400	1.576	1.214	1.138	0.515	0.271	0.131	0.148
Slow *vs.* fast phase lag (deg)								
α (fitted)	88.15	101.83	154.71	172.93	194.93	227.96	273.83	290.72
α (Δt = 34.99 ms)	100.77	138.56	163.75	176.35	188.95	201.54	214.14	226.74
Phase change per decade (deg per log scot. td)								
ϕ (fitted)	16.88	51.61	46.64	47.67	48.82	42.66	46.05	49.35
ϕ (t_{10} = 9.61 ms per log scot. td)	27.68	38.06	44.97	48.43	51.89	55.35	58.81	62.27
Absolute phase delay (deg)								
ω (fitted)	343.99	484.79	605.18	662.41	702.38	768.59	814.23	855.09
ω (t_{abs} = 129.80 ms)	373.82	514.01	607.46	654.19	700.92	747.65	794.38	841.10

where R is the response, R_{max} is the maximum possible response, I is the time-averaged intensity, and σ is the half-saturation constant. This function has been used before to describe the ERG *b*-wave response (Fulton & Rushton, 1978; Arden et al., 1983; Peachey et al., 1989).

We further assume that the signals produced by the Ganzfeld flickering stimuli, which were flickered at 100% contrast, are temporally filtered before they reach the saturating stage represented by eqn. (4) to yield two components: a flickering component equivalent to a time-averaged intensity of I_f, and a steady component equivalent to a time-averaged intensity of I_s. Using eqn. (4), we can compute the response, R_f, to the flickering component, I_f, by subtracting the response to the steady component, I_s, from the response to the combined steady and the flickering components, $I_f + I_s$, to give (see Williams & Gale, 1977):

$$R_f = \frac{\sigma I_f R_{max}}{(I_s + \sigma)^2 + I_f(I_s + \sigma)} \quad (5)$$

To implement this equation, we have assumed that the sum of the time-averaged intensities, I_f, and I_s is equal to I, so that in eqn. (5) we can substitute Ix for I_f and $I(1 - x)$ for I_s, where x is the stimulus modulation ($0 \leq x \leq 1$) at the saturating stage. Thus,

$$R_f = \frac{\sigma I x R_{max}}{[I(1 - x) + \sigma]^2 + Ix[I(1 - x) + \sigma]} \quad (6)$$

(We note that because the flicker waveform is a series of brief pulses, the *signal* modulations are, in fact, twice the stimulus modulations.)

The values for σ were obtained by an iterative procedure in which, given initial estimates for the other parameter values, σ was varied in ~0.1 scot. td steps to find the best fit between the amplitude data and the model prediction. In accordance with the observation that the phase transition and null occur at approximately the same intensity (Sharpe et al., 1989; Stockman et al., 1991; and see Figs. 6 and 7, above), we assumed that the half-saturation constant was independent of frequency. For the normal observer (Table 1), σ was found to be 0.7 scot. td, and for the achromat (Table 2) 0.4 scot. td.

The choice of R_{max} was fairly arbitrary, since we could vary either x or R_{max} to alter the height of the saturating function in order to align it with the low intensity portion of the response–intensity function defined by eqn. (3). The value for R_{max} was set at 96.15 μV for the normal and at 100.30 μV for the achromat. These values produced a modulation x of 0.500 at 8 Hz, consistent with a two times loss of flicker modulation sensitivity at 8 Hz relative to low frequencies (see Sharpe et al., 1989, Fig. 5).

Once we had determined R_{max} and σ, we varied x, iteratively, to align the saturating function [eqn. (6)] with the low intensity response–intensity function [eqn. (3)]. The nature of this composite fit is illustrated in Fig. 15 for the normal observer: the linear portions of each function are determined by eqn. (3) and the bell-shaped portions by eqn. (6); the final composite response–intensity curves are marked by the small symbols. Tables 1 and 2 give the parameter values for both observers. The decline of x with frequency is consistent with a low pass temporal frequency response (see Conner, 1982; Sharpe et al., 1989; and Fig. 15, above). Figs. 9 and 11, above, show the model's prediction of the slow signal amplitudes for both observers (dashed lines) fitted to the amplitude data (symbols).

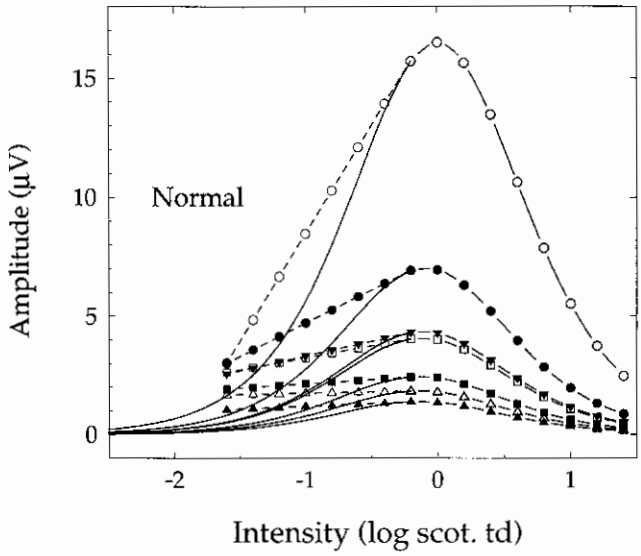

Fig. 15. Our composite method of modeling the dependence of the amplitude of the slow rod signal on intensity. At low intensities, the data are modeled by eqn. (3), which produces a linear growth in signal amplitude with the logarithm of intensity (dashed lines). At higher intensities, the data are modeled by eqn. (6), which is a hyperbolic saturation function (continuous lines). The composite functions that were used to model the slow rod signals in the normal observer are indicated by the symbols. A similar method was used for the achromat observer (not shown).

Implicit in the use of eqn. (6) is the assumption that the saturation constant (σ) of the slow signal is independent of frequency. Thus saturation is assumed to depend only on the time-averaged intensity, and is independent of the amplitude of the flicker signal that is transmitted to the saturating site (which will vary with frequency). It would have been straightforward to have made the saturation frequency-dependent by interposing a nonlinearity before the saturating site, but the ERG data (see Figs. 9 and 11) are consistent with the idea that the saturation is roughly independent of frequency.

Premise #4: The fast rod signal (R_f) grows linearly with intensity

The response of the fast signal is modeled by

$$R_f = kI \quad (7)$$

where k is a scaling constant. The values of k were obtained by a best-fitting procedure in which the least-squares logarithmic difference between the model predictions and the ERG amplitudes was found. We adopted a *logarithmic* least-squares best-fitting criterion *for this fit only* in order to reduce the influence of large signal amplitudes (at high intensities), which distort the fit in the region of the null, where the amplitudes are small. We used eqn. (2), assuming our estimate of the slow signal response–intensity function [see Premises #2 and 3, eqns. (3) and (6)] and assuming a preliminary estimate of $\Delta\theta$ based

on a difference in time delay (Δt) between the slow and fast rod signals [see Premise #5, eqn. (8a), below], to find the best-fitting values of k at each frequency. These new values of k were then used to revise our best-fitting estimate of Δt (and also t_{abs} and t_{10}; see Premise #6). Finally, the entire procedure was repeated once again to produce the values of k given in Table 1 for the normal and in Table 2 for the achromat. The model's prediction of the fast signal amplitudes are shown in Figs. 9 and 11 (dotted-dashed lines).

Premise #5: There is a time delay between the slow and fast rod signals

We assume a difference in time delay between the two signals of Δt ms, so that the phase difference ($\Delta\theta$) between the slow and fast signals can be calculated as

$$\Delta\theta = 0.36\Delta t\nu \tag{8a}$$

where ν is the frequency in Hertz. In addition to assuming a fixed time delay between the two signals, we also fitted $\Delta\theta$ independently at each frequency (see Premise #6).

The alternative formulation (see Fig. 15) in which the fast signal is assumed to be inverted in sign (i.e. phase shifted by 180 deg) with respect to the slow signal is

$$\Delta\theta = -180 + 0.36\Delta t\nu \tag{8b}$$

Premise #6: The rod system is subject to a time delay that declines linearly with log_{10} intensity

We assume that, in addition to the transition from a slow to a fast rod signal, there is an intensity-dependent reduction in the phase delay ($\theta_{\log I}$) for both signals *together* that can be approximated by assuming that there is a reduction in time delay (t_{10}) that is linear with log intensity. Thus,

$$\theta_{\log I} = \theta_{10} log\, I = 0.36\nu t_{10} \log I \tag{9}$$

where ν is the frequency in Hertz, t_{10} is the reduction in time delay in milliseconds per decade of intensity, θ_{10} is the reduction in phase delay in degrees per decade of intensity, and I is the intensity in scot. td.

Finally, to account for the absolute phase delays of the system (θ_{abs}), we propose that

$$\theta_{abs} = 0.36\nu t_{abs} \tag{10}$$

where t_{abs} is a constant time delay that is added at all intensities.

The overall phase delay of the rod system (ϕ) is

$$\phi = \theta_{abs} + \theta_{\log I} - \arctan\left(\frac{r \sin\Delta\theta}{1 + r\cos\Delta\theta}\right) \tag{11}$$

Relying upon initial estimates of r (see Premises #2–4), we obtained the final values of θ_{abs}, θ_{10}, and $\Delta\theta$ in two ways.

First, we substituted eqns. (8–10) in eqn. (11), and found the best-fitting single values of t_{abs}, t_{10}, and Δt. Then, using this new estimate of Δt, we redetermined the best-fitting values of k [the scaling constants for the fast signal—see eqns. (2) and (7)], and lastly, using the revised values of k, we redetermined the best-fitting values of t_{abs}, t_{10}, and Δt. For the normal and achromat, respectively, these values were 116.70 and 129.94 ms for t_{abs}; 10.76 and 9.50 ms per $\log_{10}$ scot. td for t_{10}; and 33.53 ms and 35.70 ms for Δt. Tables 1 and 2 give the final values converted to phase angles at each frequency.

In the second method, we used the final values of r obtained by the first method and found the best-fitting values of θ_{abs}, θ_{10} [see eqn. (9)] and $\Delta\theta$ individually at each frequency [i.e. we ignored eqns. (8) and (10) and substituted $\theta_{10} \log I$ for $\theta_{\log I}$]. The results are given in Table 1 for the normal observer and in Table 2 for the achromat. This analysis provided us with an indication of how the rod system deviates from a model that incorporates only fixed and variable time delays that are independent of frequency.